Coupled Ocean–Atmosphere Dynamics in a Simple Midlatitude Climate Model

DAVID FERREIRA AND CLAUDE FRANKIGNOUL

Laboratoire d'Océanographie Dynamique et de Climatologie, Unité mixte de recherche CNRS-ORSTOM-UPMC, Université Pierre et Marie Curie, Paris, France

JOHN MARSHALL

Program in Atmospheres, Oceans, and Climate, Department of Earth, Atmospheric and Planetary Sciences, Massachusetts Institute of Technology, Cambridge, Massachusetts

(Manuscript received 22 February 2000, in final form 16 January 2001)

ABSTRACT

Midlatitude air–sea interactions are investigated by coupling a stochastically forced two-layer quasigeostrophic channel atmosphere to a simple ocean model. The stochastic forcing has a large-scale standing pattern to simulate the main modes of low-frequency atmospheric variability. When the atmosphere interacts with an oceanic mixed layer via surface heat exchanges, the white noise forcing generates an approximately red noise sea surface temperature (SST) response. As the SST adjusts to the air temperature changes at low frequency, thus decreasing the heat flux damping, the atmospheric spectra are slightly reddened, the power enhancement increasing with the zonal scale because of atmospheric dynamics. Decadal variability is enhanced by considering a first baroclinic oceanic mode that is forced by Ekman pumping and modulates the SST by entrainment and horizontal advection. The ocean interior is bounded at its eastern edge, and a radiation condition is used in the west. Primarily in wintertime conditions, a positive feedback takes place between the atmosphere and the ocean when the atmospheric response to the SST is equivalent barotropic. Then, the ocean interior modulates the SST in a way that leads to a reinforcement of its forcing by the wind stress, although the heat flux feedback is negative. The coupled mode propagates slowly westward with exponentially increasing amplitude, and it is fetch limited. The atmospheric and SST spectral power increase at all periods longer than 10 yr when the coupling with the ocean interior occurs by entrainment. When it occurs by advection, the power increase is primarily found at near-decadal periods, resulting in a slightly oscillatory behavior of the coupled system. Ocean dynamics thus leads to a small, but significant, long-term climate predictability, up to about 6 yr in advance in the entrainment case.

1. Introduction

There has been growing interest in understanding the nature of the air–sea interactions controlling extratropical sea surface temperature (SST) variability on climatic timescales. As reviewed by Frankignoul (1985), the interannual SST anomalies mainly reflect the response of the oceanic surface mixed layer to the day-to-day changes in the local air–sea fluxes, which act as a stochastic forcing. Away from frontal zones, the main SST anomaly forcing is by surface heat exchanges and vertical entrainment, and turbulent heat fluxes also contribute to SST anomaly damping (Frankignoul et al. 1998). Although the decay time of the SST anomalies is typically 3 months, that of the heat content in the mixed layer is longer and wintertime SST anomalies generally recur during the following autumn (Alexander and Deser 1995). As discussed by Deser and Blackmon (1993), the decadal SST fluctuations in the North Atlantic are related to the wintertime atmospheric anomalies in broadly the same way as on shorter timescales, with stronger winds overlying cooler SSTs, while different relations are seen on interdecadal and longer timescales. Halliwell and Mayer (1996) showed that in the westerlies local anomalous turbulent heat flux is effective in forcing the wintertime SST anomalies down to the decadal period, although in the western North Atlantic, the geostrophic variability strongly modulates the SST fluctuations (Halliwell 1998). The decadal signal may have an enhanced variance around periods of about 12–14 yr (Deser and Blackmon 1993; Sutton and Allen 1997), but a dominant SST timescale does not require an active ocean–atmospheric coupling; it could arise through the interplay between stochastic atmospheric forcing with a fixed spatial pattern and oceanic advection (Saravanan and McWilliams 1998), or reflect SST modulation by stochastically forced geostrophic fluctuations (Frankignoul et al. 1997; Jin 1997).

General circulation model (GCM) experiments with

Corresponding author address: Claude Frankignoul, Laboratoire d'Océanographie Dynamique et de Climatologie, Unité mixte de recherche CNRS-ORSTOM-UPMC, Case 100, Université Pierre et Marie Curie, 4 place Jussieu, 75252 Paris, France.
E-mail: cf@lodyc.jussieu.fr

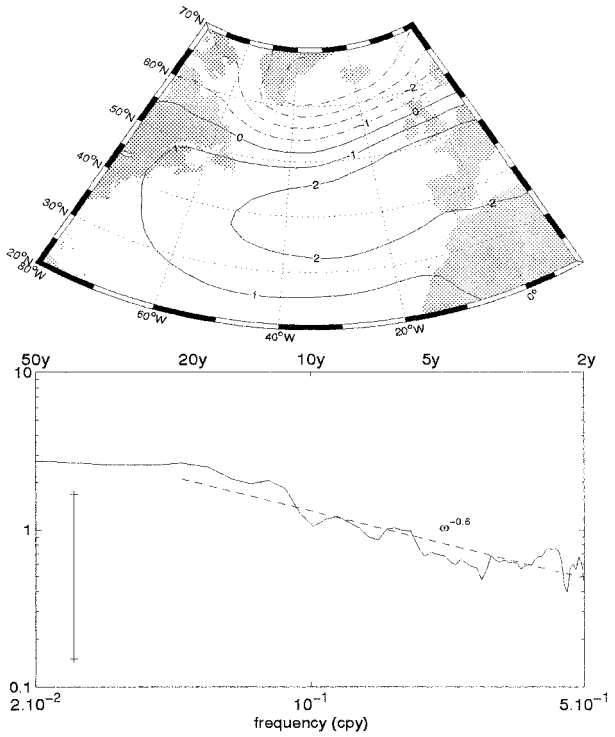

FIG. 1. (top) NAO pattern obtained as the leading mode (47% of the variance) of wintertime sea level pressure over the North Atlantic from an EOF analysis. Monthly anomalies were computed from the NCEP reanalysis for the period 1948–99 and then averaged to form wintertime (Dec–Mar) anomalies. (bottom) The power spectrum (arbitrary units) of the first principal component was computed using the multitaper method. The power law in dashed line was obtained by a least squares fit for periods between 2 and 20 yr.

prescribed SST anomalies generally suggest that there is some atmospheric response in fall and winter, but it is model dependent. For example, in Kushnir and Held (1996), the response to a North Atlantic SST anomaly is very weak and baroclinic, while in Palmer and Sun (1985), Ferranti et al. (1994), and Peng et al. (1995), it is stronger and equivalent barotropic, the SST anomaly primarily displacing the storm track and altering the upper-tropospheric eddy vorticity flux. Rodwell et al. (1999) showed that much of the observed low-frequency variability of the North Atlantic oscillation (NAO) can be reproduced by an atmospheric GCM forced by the observed changes in SST and sea ice. In addition, Czaja and Frankignoul (1999) showed that North Atlantic SST anomalies have an impact on the observed atmospheric variability in late spring and early winter. These studies suggest that the ocean could lead to a small predictability of the wintertime NAO, consistent with the slight redness of its spectrum discussed in Hurrel and van Loon (1997) and Wunsch (1999). The NAO redness is illustrated in Fig. 1, where the spectral slope is slightly steeper than in Wunsch (1999) because the NAO is defined by a large-scale pattern rather than by the traditional NAO index.

Decadal oscillations sustained by a positive midlatitude ocean–atmosphere feedback were invoked by Latif and Barnett (1994) to explain decadal variability in the North Pacific in the ECHO coupled general circulation model. In their scenario, in an anomalously strong subtropical gyre, the Kuroshio transports more warm water northward and increases the SST in the western and central Pacific. The atmospheric response to the SST anomaly is such that it sustains the latter via a positive heat flux feedback while decreasing the wind stress curl, which after some delay spins down the subtropical gyre and eventually yields a SST anomaly of the reversed sign. Grötzner et al. (1998) have suggested that a similar coupling is at play in the North Atlantic. However, the midlatitude ocean is less active in ECHAM1/LSG and the heat flux feedback negative (Zorita and Frankignoul 1997; Frankignoul et al. 2000), and the ocean is primarily passive in the Geophysical Fluid Dynamics Laboratory model (Delworth 1996). Since cause and effect are difficult to distinguish in coupled simulations, more studies are needed to understand the nature of the air–sea coupling and establish statistical signatures that could be tested with observed or coupled model data.

Early basic studies of the midlatitude coupling have been reviewed by Frankignoul (1985) and Barsugli and Battisti (1998). The latter coupled a stochastically forced slab (or energy balance) atmosphere to a slab ocean via surface heat exchanges. The coupling allowed for an adjustment between air temperature and SST that reduced the heat flux feedback at low frequencies, enhancing the oceanic and atmospheric variability (see also Saravanan and McWilliams 1998). Longer timescales are introduced in the coupled system by the ocean dynamics. Frankignoul et al. (1997, hereafter FMZ) showed that the baroclinic response of the ocean to stochastic wind stress forcing was red with a decadal dominant timescale, and Jin (1997) that the geostrophic currents distorted the climatological SST gradient, leading (for realistic SST damping time) to a very weak decadal peak under a spatially organized wind stress forcing, and a more pronounced one with active atmospheric coupling. However, the coupling was based on ad hoc assumptions for the zonally averaged quantities. A balance between meridional wind anomalies and low-level convergence, plus the assumption that the latter is proportional to the SST perturbation, was used instead by White et al. (1998) to study the wind stress feedback upon free oceanic Rossby waves. Empirical coupling approaches have also been used, as in Weng and Neelin (1998) and Neelin and Weng (1999), who used the response of atmospheric GCMs to prescribed SST to specify the wind stress and heat flux feedback acting on SST anomaly, or in Xu et al. (1998), who coupled an oceanic GCM to a statistical atmosphere derived from a coupled GCM, although this procedure biases air–sea fluxes toward positive feedback (Frankignoul 1999). A dynamically more consistent approach, albeit simple enough to be tractable analytically, was used by Goodman and

TABLE 1. Standard value of the parameters.

β	1.8×10^{-11} m^{-1} s^{-1}
f	8×10^{-5} s^{-1}
c_o	-2 cm s^{-1}
L_a	700 km
ρ_a	1.3 kg m^{-3}
ρ_o	10^3 kg m^{-3}
C_{po}	4×10^{-6} kg m^{-3} K^{-1}
H_a	10 km
H_o	4500 m
C_D	1.5×10^{-3}
γ_r	1.5×10^{-6} s^{-1}
γ_a	4×10^{-6} s^{-1}
γ_s	1×10^{-7} s^{-1}
γ_e	3×10^{-8} s^{-1}
U_1	18 m s^{-1}
U_2	7 m s^{-1}
k	4×10^{-7} m^{-1}

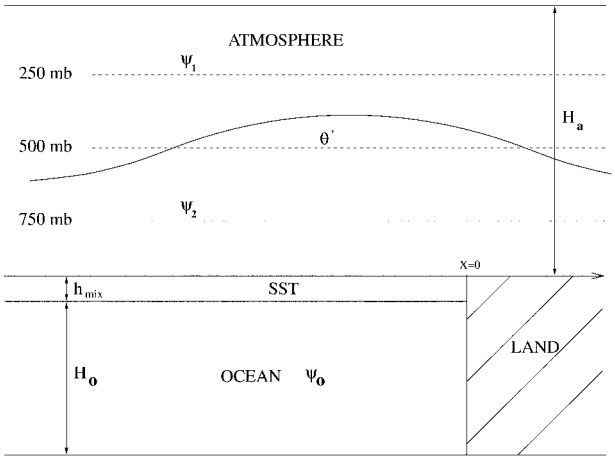

FIG. 2. Schematic longitude–height cross section of the coupled ocean–atmosphere system.

Marshall (1999, hereinafter GM), who coupled a two-layer quasigeostrophic channel atmosphere to a baroclinic oceanic Rossby wave via an oceanic mixed layer, and showed that the wind stress curl feedback could lead to growing coupled modes. However, the calculation was done for an unbounded ocean. On the other hand, the western boundary current plays a key role in the simple models of Cessi (2000) and Marshall et al. (2001), with linear dynamics and simple parameterizations relating its fluctuations to heat transport.

The goal of the present paper is to refine GM's model by taking into account some of the effects of the finite width of the ocean, which limits the growth of the coupled perturbations, and use FMZ's statistical approach to quantitatively estimate the decadal variability that results from the natural variability of the weather forcing. For algebraic simplicity, we only consider large atmospheric zonal scales and linear perturbations to a basic oceanic state at rest, which is a reasonable approximation for the first baroclinic mode (Sirven and Frankignoul 2000), and we do not represent the western boundary current, using instead a radiation condition. The focus is thus on the air–sea coupling in the central and eastern parts of an ocean basin, admittedly a severe limitation. The coupled model is formulated in section 2. The response of the atmospheric model to prescribed SST is discussed in section 3 and the coupling with the oceanic mixed layer in section 4. The SST modulation by interior motions is taken into account in section 5. The influence of the wind stress feedback onto the oceanic and atmospheric spectra is discussed in section 6 and some statistical signature of the air–sea interaction documented. Conclusions are presented in section 7.

2. A simple coupled model

Our simple coupled model can be succinctly stated by three equations for our three main variables, θ the atmospheric temperature anomaly, T the SST anomaly, and ψ_o the ocean interior geostrophic streamfunction anomaly (these are derived from first principles in appendix A):

atmosphere:

$$(\Gamma_T + V\partial_x)\theta = \Gamma_a T + F \tag{1}$$

sea surface temperature:

$$\partial_t T = \gamma_e(T_o - T) + \gamma_s(\theta - T) + Q_o \tag{2}$$

ocean:

$$\frac{1}{c_o}\partial_t\psi_o + \partial_x\psi_o = -\alpha\psi_s, \tag{3}$$

where T_o is the ocean interior (thermocline) temperature anomaly; ψ_s is the atmospheric streamfunction at the surface, to which the stress blowing over the ocean is proportional; c_o is the speed of first baroclinic oceanic Rossby waves; and the Γs and γs are inverse thermal timescales. Other parameters are defined below. A schematical representation of the model is given in Fig. 2.

The atmospheric model from which (1) is derived—see appendix A—is a steady two-level quasigeostrophic β-plane atmosphere linearized about a mean zonal wind with vertical shear. The transient response of the atmosphere is neglected assuming equilibrium on the timescales we are interested in. The atmosphere loses heat to the ocean mixed layer at the rate Γ_a and includes a radiative damping at the rate Γ_r ($\Gamma_T = \Gamma_a + \Gamma_r$). Atmospheric dynamics is encapsulated in V, the Doppler-shifted phase speed of a free Rossby wave in the atmosphere, a rather complicated function of the mean winds, β, the meridional wavelength, and stratification [see (A14)]. Resonance occurs for $V = 0$ when horizontal advection of heat exactly balances adiabatic heating, so that only dissipation and surface heat exchanges limit the amplitude. The stochastic forcing F represents the (white noise) forcing of temperature by baroclinic

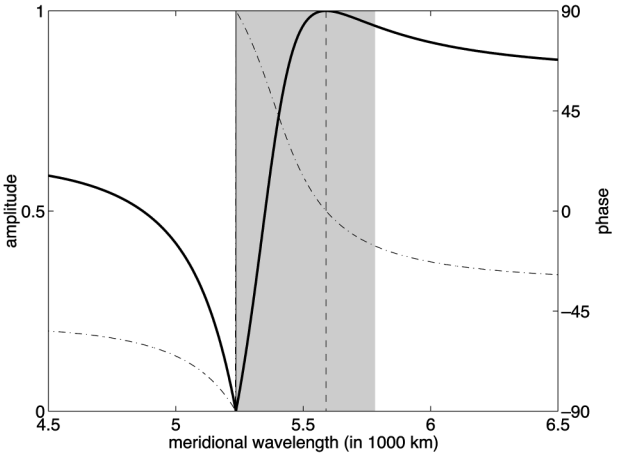

FIG. 3. Amplitude (thick solid) and phase (dashed–dotted) of the air temperature response to fixed SST anomalies as a function of the meridional wavelength l (for zonal wavenumber 2). The amplitude is normalized so that it is 1 at resonance. A negative phase corresponds to $V > 0$ and a downstream response. The vertical solid and dashed lines denote barotropicity and resonance, respectively. Shading corresponds to equivalent barotropic conditions.

eddies. Therefore, in this model, the atmosphere has a white spectrum in the absence of air–sea interaction, and redness only appears through thermal damping (section 4) or active air–sea coupling (section 5). Consistent with observations of low-frequency large-scale atmospheric modes such as NAO (see Fig. 1), we have assumed in (1) that the zonal scale is much larger than the meridional one—see (A8).

The SST anomaly can be changed by air–sea fluxes at the rate γ_s^{-1}, by entrainment of thermocline water of temperature T_o at the rate γ_e^{-1} and by horizontal advection of mean SST by geostrophic meridional current anomalies, Q_o.

The ocean is assumed to exist in a semi-infinite domain bounded to the east by land (in $x = 0$) where there is a no-normal flow condition (see Fig. 2). There are no western boundary currents and we impose a radiation condition in the west. The ocean interior variability is governed by first baroclinic Rossby waves excited by winds ψ_s. According to our simple atmospheric model—see (A15)—the surface winds are related to the atmospheric temperature θ through the relation:

$$\psi_s = -m\theta, \tag{4}$$

where m is a function of the mean zonal winds and controls the relative strength of the barotropic and baroclinic modes. The thermocline temperature T_o is assumed to result from the adiabatic undulation of the isopycnal surfaces underneath the mixed layer and thus can be related to the baroclinic streamfunction ψ_o:

$$T_o = r_o\psi_o, \tag{5}$$

where r_o is an appropriate scaling factor—see (A17). The source Q_o due to advection can also be related to ψ_o—see (A18):

$$Q_o = ar_o\frac{\partial\psi_o}{\partial x}. \tag{6}$$

Since the dominant modes of natural variability of the atmosphere at low frequency have a geographically fixed spatial pattern that is not sensitive to SST forcing, we represent the stochastic forcing as a standing pattern:

$$\tilde{F} = C_k(w)e^{-i\omega t}\sin(kx + \varphi)\sin(ly), \tag{7}$$

where ω is frequency, k is zonal wavenumber, l is meridional wavenumber, φ is the phase at the eastern boundary, and C_k is the amplitude. To mimic the NAO (Fig. 1), we choose $k = 4 \times 10^{-7}$ m^{-1} (zonal wavenumber 2) as standard parameter, and φ is determined for each l to obtain a well-located peak at $x = -2000$ km for $\tilde{\psi}$, as sketched in Fig. 2 (see also Fig. 11, bottom). The observations suggest that the meridional wavelength $\lambda_y = 2\pi/l$ should be on the order of 6000 km, satisfying condition (A8). The forcing is a stationary random process with zero mean and we assume that the frequency spectrum of F is white at low frequency.

Note that

- setting $T_o = Q_o = 0$ in (2), the oceanic interior motions have no influence on the atmosphere, as in FMZ;
- the interplay between the free atmosphere and the oceanic surface layer is a generalization of Barsugli and Battisti (1998) or Saravanan and McWilliams (1998), who assume $V\partial_x\tilde{\psi} = 0$ (no atmospheric dynamics) and $\gamma_e = 0$ (no entrainment); and
- our equations for the ocean, atmosphere, and coupling physics are those of GM, except for the inclusion of a stochastic forcing and a radiative damping in the atmosphere.

3. The atmospheric response to a fixed SST anomaly

To understand the role of atmospheric dynamics, it is interesting to first study the response of the atmosphere to a fixed SST anomaly. Assuming an e^{ikx} form for the latter and neglecting the stochastic forcing, (1) can be solved for θ:

$$\theta = \Gamma_a\frac{T}{\Gamma_T + iVk}, \tag{8}$$

and the surface wind response is given by (4). The transfer function between T and θ has an imaginary part, which results in a zonal phase shift. Figure 3 illustrates the amplitude and phase of the response as a function of l for zonal wavenumber 2; shading denotes meridional wavelength for which the atmosphere is equivalent barotropic (atmospheric fluctuations have the same sign throughout the atmosphere and increasing amplitude with height). For $V > 0$, the phase is negative and the atmospheric response is shifted downstream of the SST while it shifted upstream for $V < 0$.

The amplitude of the air temperature response de-

pends on the relative size of the thermal equilibration timescale Γ_T^{-1} and the advective-propagative timescale $(Vk)^{-1}$ (the time for a free Rossby wave to travel a distance k^{-1}). At resonance ($V = 0$ and $l = 2\pi/5590$ km for our standard parameters in Table 1), the forced response is maximum and in phase with SST (vertical dashed–dotted line in Fig. 3). Near resonance, one has $Vk \ll \Gamma_T$, that is the thermal equilibration time is much shorter than the advective-propagative time, and the air temperature adjusts closely to the SST. This corresponds to the thermal equilibration discussed by Shutts (1987), Marshall and So (1990), and GM. In this limit, the atmospheric response is equivalent barotropic, a warm high (cold low) settles over a warm (cold) SST anomaly. Away from resonance, for Vk/Γ_T large, the atmospheric response is smaller and zonally shifted from the SST anomaly (the forced response limit of Shutts 1987). Near barotropicity ($V = \infty$ and $l = 2\pi/5236$ km^{-1}), the air temperature anomaly vanishes and the forced response is minimum.

The phase of the forced surface pressure is easily obtained from Fig. 3 noting that air temperature (or wind shear) and surface pressure anomalies have the same sign only for equivalent barotropic conditions, otherwise they are in quadrature.

4. Thermal coupling between the atmosphere and the mixed layer

We first neglect the SST modulation by wind-driven geostrophic currents in the ocean. Above the ocean, (1) holds while the SST Eq. (2) reduces to (setting $T_o = Q_o = 0$):

$$T = \frac{\gamma_s}{\gamma_{To} - i\omega}\theta = b\theta, \tag{9}$$

where $\gamma_{T_o} = \gamma_s + \gamma_e$ is the (inverse) damping timescale of SST anomalies, and $b(\omega)$ is a transfer function between θ and T that describes the frequency dependence of the coupling between SST and the atmosphere. It is understood that $\theta = \theta(x, \omega)$ and $T = T(x, \omega)$ are Fourier components.

Replacing in (1) yields:

$$\left(\Gamma + V\frac{\partial}{\partial x}\right)\theta = C_k \sin(kx + \varphi), \tag{10}$$

where $\Gamma = \Gamma_T - b\Gamma_a = (1 - b)\Gamma_a + \Gamma_r$. Since the steady-state assumption prevents baroclinic instability, the solution consists of a free mode plus a forced solution. The free mode varies like $\exp(-\Gamma x/V)$ and propagates with a varying amplitude since Γ is complex. The forced solution is given by

$$\theta = \frac{C_k}{(Vk)^2 + \Gamma^2}[\Gamma \sin(kx + \varphi) - Vk \cos(kx + \varphi)] \quad \text{for } x < 0. \tag{11}$$

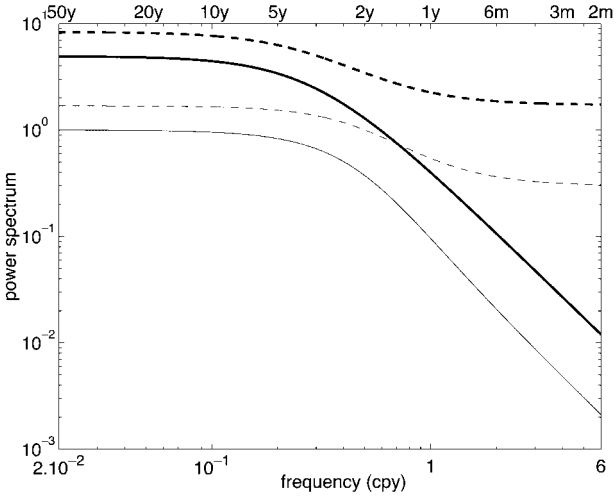

FIG. 4. Power spectra of SST (solid lines) and air temperature (dashed lines) at $x = -4000$ km when there is no mixed layer modulation by the geostrophic fluctuations. Forcing is at zonal wavenumber 2 with $\lambda_y = 5400$ km (thin lines) and $\lambda_y = 5600$ km (thick lines). Plots have been made by (arbitrarily) choosing that the low-frequency spectral level of SST for $\lambda_y = 5400$ km is one.

Above land ($x > 0$), the solution is obtained taking $\Gamma_a = 0$ in (11) and there is no propagation. To match the solutions at $x = 0$ and remain bounded, the free mode must be added above either land or ocean, depending on the sign of V. However, the free solution has a zonal decay scale that is too short for the approximation (A8) to remain valid. Rather than using the full set of equations, which would require tedious algebra involving a scale of the order of the Rossby radius, we simply neglect the free solutions and use (11) above the ocean but recognize that the solution breaks down close to the eastern boundary.

If the frequency spectrum of the air temperature θ were white, then (9) would reduce to the first-order Markov process considered by Frankignoul and Hasselmann (1977). The system (9)–(10) is similar the one discussed by Barsugli and Battisti (1998), except for the inclusion of explicit atmospheric dynamics. As in their study, the atmospheric spectrum $S_\theta(\omega)$, which is easily computed from (11), is not white because of the air–sea temperature adjustment. As illustrated in Fig. 4 (dashed lines), $S_\theta(\omega)$ is white for $\gamma_{T_o} \ll \omega$, then it increases as frequency decreases because the SST starts adjusting to the air temperature anomaly and reduces the air–sea contrast and thus the heat flux. For $\omega \ll \gamma_{T_o}$, the spectrum becomes white again, but at a higher level since the SST is fully adjusted. Correspondingly, the surface heat flux spectrum (not shown) decreases at low frequency toward a lower white noise level. The SST anomaly spectrum (Fig. 4, solid lines), computed from (9), broadly resembles that of a first-order Markov process, although the air–sea adjustment, and thus the reduced thermal damping, has resulted in an increased persistence of both air temperature and SST anomalies.

Note that the spectra have been estimated at $x = -4000$ km for comparison with the coupled case, but the spectral shape depends little on x. However, because of (7) the spectral level varies strongly in the zonal direction (see Fig. 11, section 6a).

The power enhancement $E = S_\theta(0)/S_\theta(\gamma_{T_o} \ll \omega)$ of θ at very low frequency is identical to the ratio of coupled-to-uncoupled low-frequency atmospheric variance. The latter is easily obtained by comparing (11) with the solution for fixed SST [i.e., with $T = 0$ in (1)]. The parameter E is a measure of the air–sea temperature adjustment at low frequency. It depends on the degree to which thermal equilibration is achieved, hence on both k and l (see section 3). For small $|Vk/\Gamma|$, thermal equilibration occurs and results in a strong air–sea temperature adjustment, hence E is large (the atmospheric spectrum is reddened). Correspondingly, the persistence of SST anomaly is long and the spectral level is high (Fig. 4, thick lines). For $Vk = 0$ (either because $k = 0$ or there is resonance), E and the persistence of SST anomaly are maximum, the latter reaching about 7 months for our standard values. For large $|Vk/\Gamma|$, the advective-propagative timescale becomes shorter, the air–sea temperature adjustment is small, and E decreases. Then, the persistence of SST anomaly is short, and the spectral level is lower (thin lines). For $Vk = \infty$ (barotropic case, no air temperature anomaly), the atmospheric spectrum is white and the persistence of SST anomaly minimum, given, as expected from (9), by $\gamma_{T_o}^{-1}$ (3 months for our standard values).

The averaged power enhancement in coupled models is about 2.5 in Manabe and Stouffer (1996); it is 1.7 in Bladé (1997). Also, the latter noticed that it was scale dependent, the lowest wavenumbers being most strongly enhanced. If we assume for simplicity an e^{ikx} dependence for all variables (which avoids the zonal nonhomogeneity caused by our choice of forcing pattern), choose $\lambda_y = 5400$ km (an intermediate value between the extreme cases $V = 0$ and $V = \infty$), and neglect γ_e (which corresponds to the above GCM experiments), we find that E decreases with increasing zonal wavenumber: $E = 13.4$, 4, 1.9, and 1.4 at zonal wavenumber 0, 1, 2, and 3, respectively ($E = 5.2$, 2.9, 1.7, and 1.3 when considering entrainment and decreases further if surface friction is added but increases if l is closer to resonance). Thus, the predictions of our simple model are broadly consistent with the GCMs. Contrary to Barsugli and Battisti (1998), our model is able to reproduce the wavenumber dependence of the power enhancement discussed in Bladé (1997). In their study, they expected ''the dynamical part of the atmospheric response to act generically as a negative feedback, with atmospheric heat fluxes partially offsetting the diabatic effects of an SST anomaly,'' which is consistent with our results. However, they parameterized it as a linear scale-independent negative feedback. Our model suggests that the wavenumber dependence of the power enhancement seen in GCMs could be due to atmospheric dynamics, namely changes in the relative importance of thermal equilibration and heat advection.

5. Fully coupled case

When SST modulation by the geostrophic motions is included, we eliminate θ and T from (1)–(6) and obtain

$$\overbrace{\left(1 + \frac{V}{\Gamma}\partial_x\right)}^{A}\overbrace{(-ik_o + \partial_x)\psi_o}^{B} - \overbrace{c(\gamma_e + a\partial_x)\psi_o}^{C} = \frac{\alpha m}{\Gamma}\tilde{F}, \tag{12}$$

where $k_o = \omega/c_o$ is the wavenumber of a free oceanic Rossby wave of frequency ω and the combination of coupling constant c is

$$c = \alpha m \frac{\Gamma_a}{\Gamma}\frac{r_o b}{\gamma_s}. \tag{13}$$

Term A represents atmospheric dynamics, term B represents Rossby wave propagation, and term C is the coupling between the thermocline and the atmosphere via the oceanic mixed layer.

The free modes of the coupled system are solutions of the homogeneous part of (12). They vary like $e^{\delta x}$ where δ must satisfy the quadratic equation:

$$\left(1 + \frac{V}{\Gamma}\delta\right)(\delta - ik_o) = c(\gamma_e - a\delta). \tag{14}$$

As expected, the two solutions δ_1 and δ_2 are an oceanic Rossby wave and the free solution of section 4, both modified by the coupling. For the same reason as above, we neglect the second solution and only keep the coupled Rossby wave, even though the atmospheric solution is then discontinuous at $x = 0$ and the solution is not valid near the eastern ocean boundary. The retained solution is obtained by adding the forced part of the solution to the coupled mode:

$$\psi_o = \alpha_1 e^{\delta_1 x} + \alpha_2 \sin(kx + \varphi) + \alpha_3 \cos(kx + \varphi), \tag{15}$$

where α_2 and α_3 are determined by injecting the solution in (12), and α_1 is then readily obtained from (A21). The geostrophic response to the stochastic forcing at each ω is thus given by a forced standing response plus a free westward-propagating one that is generated at the eastern boundary to satisfy the no-normal flow condition. The latter resembles an oceanic Rossby wave but, because of the air–sea coupling, its amplitude increases or decreases as it propagates westward, depending on the parameters. Note that an increase in amplitude corresponds to the temporal instability investigated by GM.

If the coupling is weak enough, one can derive simple expressions of the roots δ_1 and δ_2 and thus of the air–sea feedback. Details are given in appendix B.

a. Entrainment case

We first consider the SST modulation by entrainment and neglect the influence of geostrophic advection [taking $a = 0$ in (14)]. In the weak coupling case, the spatial growth or decay of the Rossby wave as it propagates westward depends on the frequency and is given by the real part of (B3). We further simplify the solution and assume that ω is sufficiently low for the SST tendency to be neglected ($\omega \ll \gamma_{T_o}$), yielding

$$\mathrm{Re}(\delta_1) = \frac{\alpha r_o}{r_a}\frac{\Gamma_a}{\Gamma}\frac{\gamma_e}{\gamma_{To}}\frac{\left(1+\frac{\mu}{2}\right)}{1+\left(\frac{Vk_o}{\Gamma}\right)^2}. \qquad (16)$$

The condition for westward growth is then:

$$1+\frac{\mu}{2} < 0 \quad \text{or} \quad \mu < -2, \qquad (17)$$

which from (A10) solely depends on l and the mean zonal wind. For a given zonal wind, only a limited range of meridional wavelength with equivalent barotropic fluctuations is unstable. Note that the zonal wavenumber and thus the phase speed are also modified by the coupling [see (B4) and Fig. 6 later].

The mode grows because a positive subsurface temperature anomaly [depressed isopycnal, see (A17)] and its associated positive SST anomaly generate a positive air temperature anomaly. In equivalent barotropic conditions, the latter is associated to an anticyclonic surface circulation that causes downward Ekman pumping and deepens the isopycnal further thus acting as a positive feedback (Fig. 5, top). On the other hand, for nonequivalent barotropic conditions, a positive air temperature results in a cyclonic surface circulation leading to negative feedback and a spatial decay of the coupled mode.

The condition (17) is similar to the instability condition of GM, except for the lack of dependence on zonal wavenumber that results from our approximation (A8). In the unbounded domain considered by GM, these were the modes that coupled with the ocean and led to temporal growth. In the present case, the modes grow from the eastern boundary, but their amplitude remains bounded because the fetch is limited.

The growth rate depends on Vk_o/Γ, hence on the degree of thermal equilibration (see section 3). Here, the advective–propagative timescale Vk_o is set by the scale k_o of the oceanic Rossby wave and hence depends linearly on ω. Thus, the largest growth rates are found at the lowest frequencies that favor thermal equilibration. Note that when approaching barotropic conditions ($\mu \to -\infty$), the ratio of surface wind to wind shear anomaly becomes very large, widely increasing the efficiency of the wind stress feedback. However, taking into account surface friction would strongly damp the response so that near-barotropic conditions are poorly represented in our model.

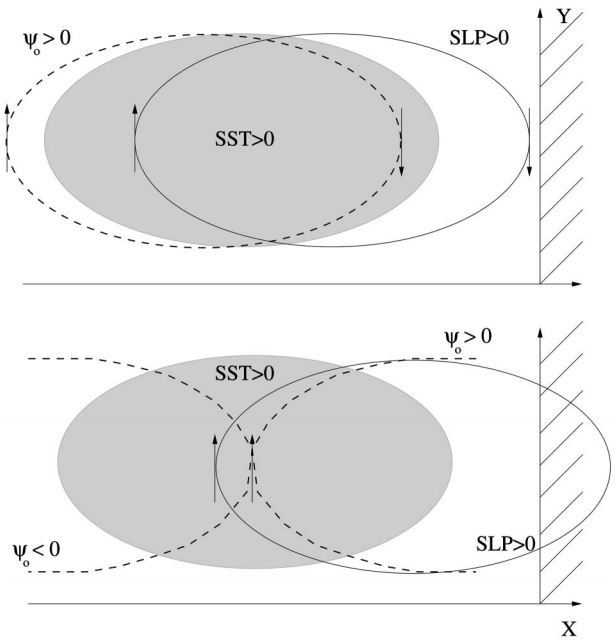

FIG. 5. Sketch of the growing coupled modes in a horizontal plane in (top) the entrainment case and (bottom) the advection case. The dashed and continuous lines represent oceanic baroclinic pressure and sea level pressure, respectively. Shading denotes a positive SST anomaly. Only a half-wavelength is represented.

Figure 6 shows the growth rate $\mathrm{Re}(\delta_1)$ (top) and the zonal wavenumber $\mathrm{Im}(\delta_1)$ (bottom) of the free modes from the exact solution of (14) as a function of ω and l for the standard values (Table 1). Relation (17) still determines the domain of significant westward growth when ω increases, so that instability primarily occurs for meridional wavelengths ranging between 5200 and 5800 km. It is thus relevant to the NAO problem. In the most unstable conditions, the instability length scale reduces to 5000 km, resulting in a large amplitude increase across an ocean basin. However, as shown below, this growth rate only pertains to winter conditions. The zonal wavenumber broadly matches that of an oceanic Rossby wave in the long-wave approximation, although it depends somewhat on l at the largest periods. In the region of strong growth rate, the zonal wavelength is indeed slightly larger resulting in an increased phase speed. Note that, because of (A8), only the low-frequency part of the figure is consistent with our simplifying assumptions. For periods shorter than about 10 years, the coupled mode should have been calculated with full atmospheric dynamics.

b. Advection case

A similar analysis can be done for the SST modulation by geostrophic advection, neglecting the entrainment term in (14). The free mode is also an oceanic

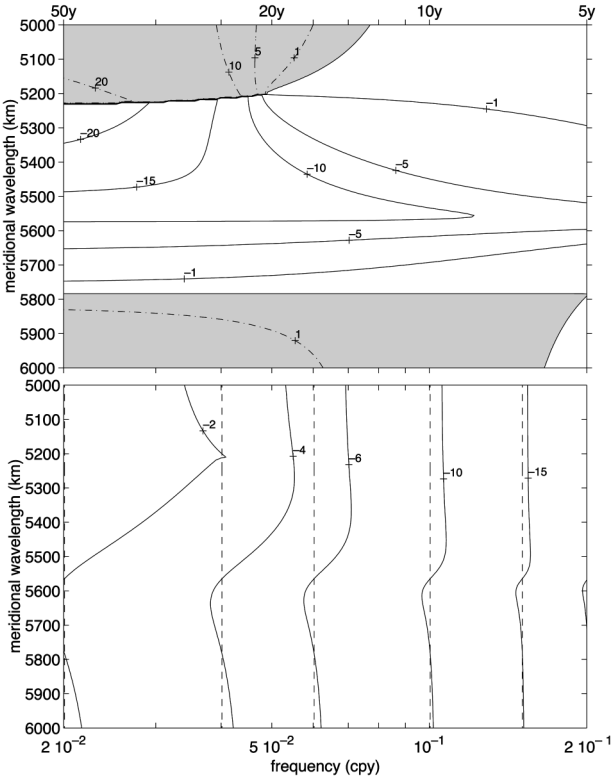

FIG. 6. (top) Contours of the growth rate (10^{-8} m^{-1}) and (bottom) zonal wavenumber (10^{-7} m^{-1}) of the coupled mode as a function of frequency and meridional wavelength for the entrainment case. Westward decay is shaded. (bottom) Dashed lines correspond to zonal wavenumber of a free Rossby wave in the long-wave approximation.

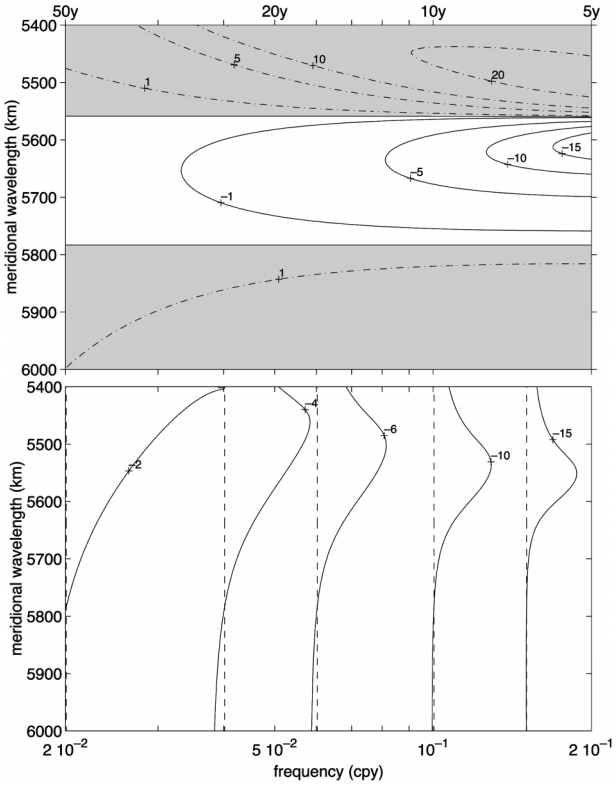

FIG. 7. As in Fig. 6 but for advection.

Rossby wave that grows or decays as it propagates westward. In the low-frequency limit, one finds from (B5):

$$\mathrm{Re}(\delta_1) = \frac{\alpha r_o}{r_a}\frac{\Gamma_a}{\Gamma}\frac{ak_o^2 V}{\gamma_{To}}\frac{1+\dfrac{\mu}{2}}{1+\left(\dfrac{Vk_o}{\Gamma}\right)^2}. \tag{18}$$

The condition for westward growth is thus

$$\left(1+\frac{\mu}{2}\right)V < 0, \tag{19}$$

and the only solution is $1 + \mu/2 < 0$ and $V > 0$. Because of the latter condition, the instability is more scale selective than in the entrainment case and westward growth only occurs for meridional wavelengths ranging between about 5600 and 5800 km. A northward flow in the ocean advects warm water from the south, creating a positive SST anomaly that, in turn, generates a positive air temperature anomaly (Fig. 5, bottom). For an equivalent barotropic atmosphere, the latter causes an anticyclonic surface circulation, hence a transfer of negative vorticity into the ocean interior. If $V > 0$, the atmospheric perturbation is downstream of the SST anomaly and it reinforces the northward SST advection, providing a positive feedback. If $V < 0$, the atmospheric perturbation is upstream of the SST anomaly, creating a southward SST advection and acting as a negative feedback. Hence, a downstream atmospheric response is necessary for growth. This is in contrast with the entrainment case where the instability could occur when the atmospheric response was shifted both east or west of the SST anomaly.

As before, a thermally equilibrated atmospheric response ($Vk_o/\Gamma \ll 1$) favors the unstable air–sea interaction. However, the strength of the coupling primarily depends on $v_o = \partial_x \psi_o$ and hence on k_o, so that the growth rate increases with frequency. Figure 7 shows the growth rate and the zonal wavenumber computed from (33) as a function of l and ω. Even without approximation, condition (19) remains approximately valid over all frequencies. The strongest growth rates are reached at high frequency and are found closer to resonance ($V = 0$) as frequency increases. Indeed, the phase shift between SST and meridional advection increases and thus provides the required phase quadrature with the mechanical forcing in conditions that become nearer to thermal equilibration. However, the zonal scale is then too short for (A8) to be acceptable (and applicable to NAO studies), so that only low frequencies (zonal wavenumber) are considered. Note that, as in the entrainment case, the zonal wavelength is larger at low frequency com-

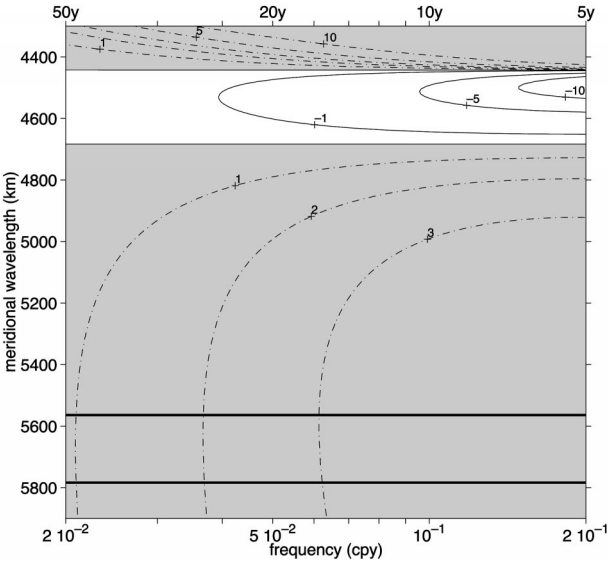

FIG. 8. (top) As in Fig. 7 but for summertime conditions. The area of westward growth rate for wintertime conditions is indicated by the two thick solid lines.

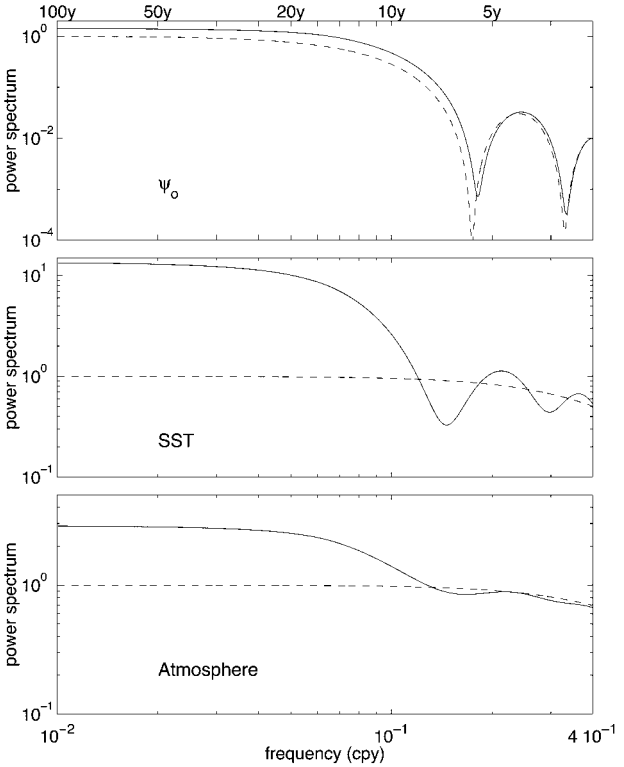

FIG. 9. Power spectra of (top) ψ_o, (middle) SST, and (bottom) air temperature for the uncoupled case (dashed line) and for the entrainment case (solid line) at $x = -4000$ km with $\lambda_y = 5400$ km.

pared to the uncoupled case, hence resulting in an increased phase speed.

c. Summer conditions

In summer conditions, the zonal flow is about one-half its wintertime counterpart, and hence we take $U_1 = 12$ m s^{-1} and $U_2 = 4$ m s^{-1}. Because of the weaker winds and the presence of a well-stratified seasonal thermocline, entrainment plays little role in the SST dynamics (Alexander and Deser 1995; Alexander and Penland 1997) and the bulk of the geostrophic modulation takes place via advection. Using $\partial_y \overline{T} = -3 \times 10^{-6}$ °C m^{-1}, $h_{\text{mix}} = 50$ m, and $\lambda = 20$ W m^{-2} K^{-1} as representative summer values, we find that the magnitude of the westward growth due to SST advection is similar to the wintertime case but is restricted to meridional wavelengths that are 20% shorter than in winter (Fig. 8). The instability thus takes place on scales that are too short to be of interest in the present context.

Note that the modes that were growing during winter are damped during summer, but the damping is very weak, nearly 1 order of magnitude smaller than the winter growth, and it can be neglected. Nonetheless, the growth rates based on winter conditions should be scaled down on a yearly basis, because of the intermittency of the instability.

6. Statistical signatures of the interaction

Realistic statistical signatures of the two-way coupling should be established by considering that the stochastic forcing has a finite wavenumber bandwidth. However, this would requires tedious integrations. Instead, we limit ourself to zonal wavenumber 2 and primarily consider two reference meridional wavelengths $\lambda_y = 5600$ km and $\lambda_y = 5400$ km that favor the advection and entrainment mechanisms, respectively. Spectra and correlations are presented for $x = -4000$ km, which is far enough from the eastern boundary to allow for a significant development of the unstable modes while remaining within the limits of a schematical Atlantic basin, away from the western boundary current region where higher-order ocean dynamics dominate and need to be represented. To clarify the statistical signature of the coupling, the spectra are shown for periods between 100 and 2.5 yr, even though (A8) is only valid for periods down to about 10 yr.

a. Power spectra

The passive response of ψ_o in the absence of SST modulation, obtained from (3), (4), and (11), provides the reference spectrum discussed in FMZ, except for the slight redness of the atmospheric forcing. The oceanic response has a red spectrum that decays as ω^{-2} at high frequency, since the ocean then responds as an integrator to the stochastic Ekman pumping, and flattens at low frequency where the fluctuations reach Sverdrup equilibrium (Fig. 9, top, dotted line). The dominant timescale (which clearly appears in the variance conserving

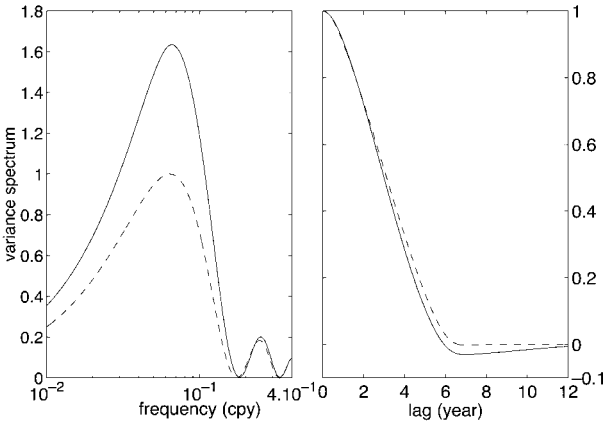

FIG. 10. (left) Variance spectrum and (right) autocorrelation of 1-yr averaged ψ_o at $x = -4000$ km with $\lambda_y = 5400$ km for a passive ocean (dashed line) and for the entrainment case (solid line). Variance has been normalized so that maximum uncoupled variance is 1.

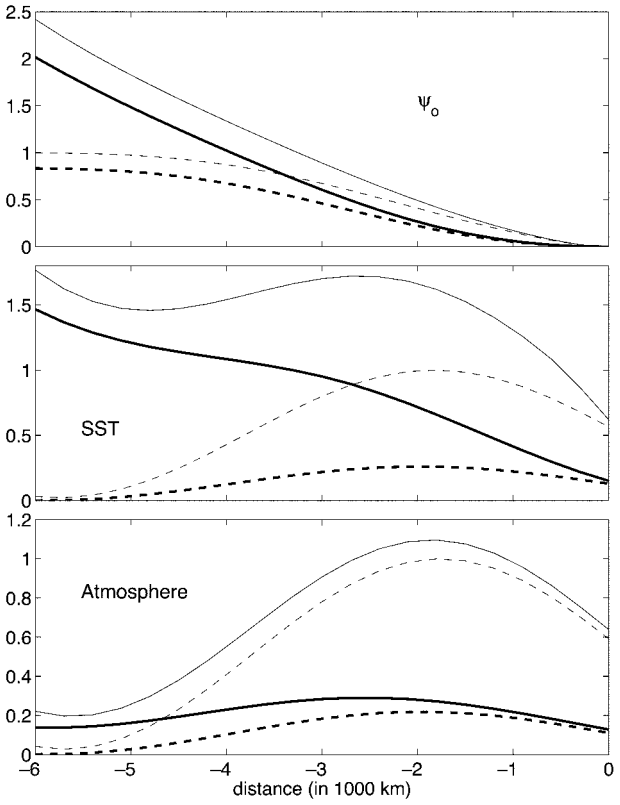

FIG. 11. Variance of (top) ψ_o, (middle) SST, and (bottom) $\tilde{\psi}$ as a function of x for a passive ocean (dashed line) and for the entrainment case (solid line) with $\lambda_y = 5400$ km. Thin (thick) line is for yearly (5 yr) averages. Normalization was made independently for each variable to have a maximum yearly averaged uncoupled variance of 1.

form in Fig. 10) is decadal and determined by the time it takes a long Rossby wave to propagate from the eastern boundary. The peaks (troughs) seen at high frequency correspond to an in-phase (out of phase) relation between the forced response and the Rossby wave generated at the eastern boundary. They are linked to our choice of a single wavenumber for the forcing and would be smoothed for a more realistic forcing pattern having a finite wavenumber bandwidth. The variance of ψ_o strongly increases westward (Fig. 11), but less so than for zonally independent forcing (FMZ) since the forcing variance peaks at 2000 km from the eastern boundary.

When the SST is modulated by entrainment, the power spectrum of ψ_o shows for our reference value $\lambda_y = 5400$ km that the positive windstress feedback enhances the power by 40% at periods larger than about 10 yr, although the dominant period remains unchanged (Figs. 9 and 10, continuous line). The enhancement depends somewhat on l (70% for $\lambda_y = 5300$ km and 40% for $\lambda_y = 5600$ km), but not the range of enhanced periods. Figure 9 compares the SST (middle) and the air temperature spectra in the absence of geostrophic fluctuations in the ocean interior (dashed line) and in their presence when the SST modulation occurs by entrainment (solid line). At low frequency, the geostrophic variability strongly enhances the power, but this primarily results from the SST modulation by the interior motions, not from the positive air–sea feedback whose relative importance is given by the ψ_o spectra. Note that the SST and $\tilde{\psi}$ spectra are little influenced by the in-phase and out-of-phase relations between free and forced ψ_o modes because ψ_o has limited power at periods shorter than decadal. Thus, our estimates remain approximately valid at high frequency even though (A8) is no longer satisfied. The influence of the geostrophic modulation on the SST spectrum is very large and sensitive to l (the enhancement factor is 13 in Fig. 9, but would be 80 for $\lambda_y = 5300$ km and 3.6 for $\lambda_y = 5600$ km). On the other hand, the atmospheric power enhancement is weaker and shows little sensitivity to l, ranging between 2.3 and 3.5; since the atmosphere responds less as it approaches the barotropic state, the larger SST enhancement has little effect. The atmospheric spectrum is thus only slightly red behaving as $\omega^{-0.5}$ at periods of several decades or less. This is consistent with the slight redness of the NAO pattern in Fig. 1, in contrast to the uncoupled case where the atmospheric spectrum became white for periods longer than 5 yr.

When the geostrophic modulation occurs via SST advection, the coupled modes for our reference value $\lambda_y = 5600$ km (close to resonance), are most unstable at high frequency so that a power enhancement is found at periods shorter than about 15 yr in the ψ_o-spectrum (Fig. 12, top), with a corresponding shift of the dominant timescale toward a shorter period (Fig. 13). As compared to the case with no geostrophic variability, coupling by advection substantially enhances the SST and $\tilde{\psi}$ spectra at periods between 10 and 20 yr (Fig. 12, middle and bottom). For the three variables, a power decrease is seen at lower frequency because the forced

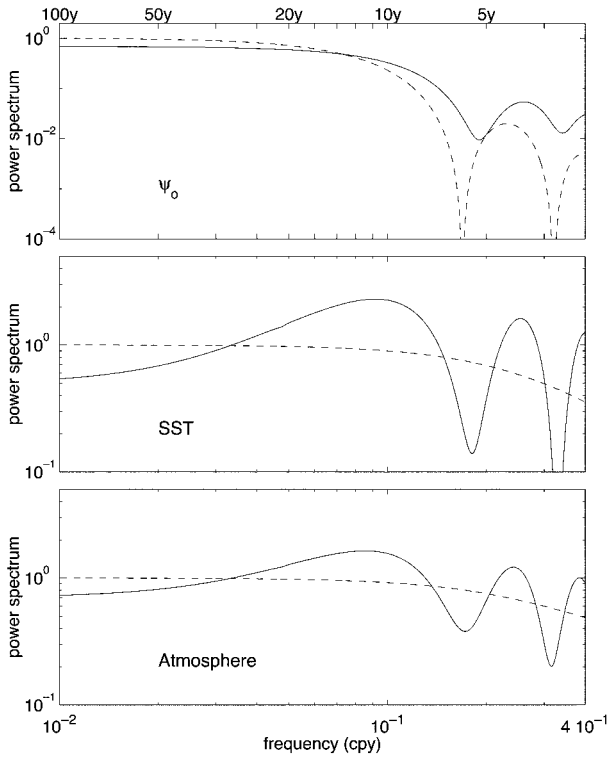

FIG. 12. As in Fig. 9, but for the SST advection case with λ_y = 5600 km.

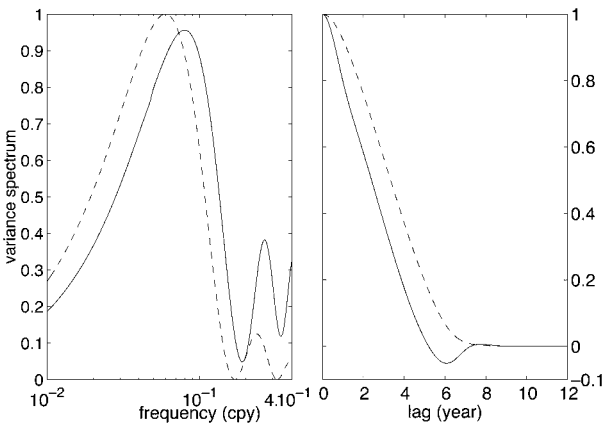

FIG. 13. As in Fig. 10 but for the SST advection case with λ_y = 5600 km.

and free modes are then slightly in quadrature, interacting negatively. However, farther away from the eastern boundary, that is, for a much larger basin than the Atlantic, a small power increase would be found instead. At high frequency, the succession of peaks and throughs seen in the SST and $\tilde{\psi}$ spectra is much more visible than in entrainment case as the meridional geostrophic velocity varies as $\omega\psi_o$ and thus has most of its variance at high frequency. As pointed out before, the high frequencies must be considered with much caution since the coupled mode then has too short a scale for (A8) to be valid. For wavelengths differing by more than a few tenth of kilometer from resonance (λ_y = 5590 km), coupling by advection would hardly affect the spectra, reflecting the narrowness of the high growth rate region in Fig. 7. Advection effects are thus only substantial near resonance. However, the amplitude of the latter in the two-layer channel model is unrealistically large (Egger 1977; Held 1983), and a more realistic atmospheric model should be used.

b. Cross correlation and atmospheric predictability

Cross-correlation functions generally provide a more stringent test of cause to effect relationships than power spectra, and they are directly linked to the predictability issue. To emphasize the long timescales, we discuss correlation based on averaged data. To do so, Fourier components have been multiplied by

$$h(\omega) = \frac{\sin(T\omega/2)}{T\omega/2}, \tag{20}$$

which is the equivalent to using a running filter of width T, with T = 1 or 5 yr. Lagged correlation is then computed from the analytical solutions by an inverse Fourier transform, assuming in addition that the stochastic forcing F is a first-order autoregressive process with a decay time ν^{-1} of 10 days (a finite energy signal). This has no effect on the spectra at the low frequencies of interest, but note that the correlations used in this section are only approximate as they are based on an integration over all frequencies while our solution for the free coupled modes is only valid for frequency shorter that decadal. This should have little impact in the entrainment case as the coupling primarily enhances the low frequencies.

For reference we first discuss the passive case of section 4 where there is no SST modulation by the geostrophic variability, only using λ_y = 5400 km as l then has very little influence on the correlations. The yearly averaged SST anomalies are somewhat correlated from one year to the next, but become uncorrelated at 2-yr interval (Fig. 14, top left, dashed line). Because of the strong SST imprint that is predicted by our simple atmospheric model, yearly air temperature anomalies have a corresponding, if slightly weaker, year-to-year persistence (Fig. 14, top right). The cross correlation between SST and surface heat flux (not shown) displays the change of sign between lead and lag conditions that is characteristic of a negative heat flux feedback (Frankignoul 1985; Frankignoul et al. 1998), whereas that between air temperature and SST (Fig. 14, bottom) peaks when SST lags by a few months, which corresponds to the 1-month lag that would be found with monthly data (Frankignoul and Hasselmann 1977). The correlation is negligible when SST leads $\tilde{\psi}$ by more than about a year, so that there is no predictive skill beyond 1 yr for the yearly averaged $\tilde{\psi}$. This corresponds to the

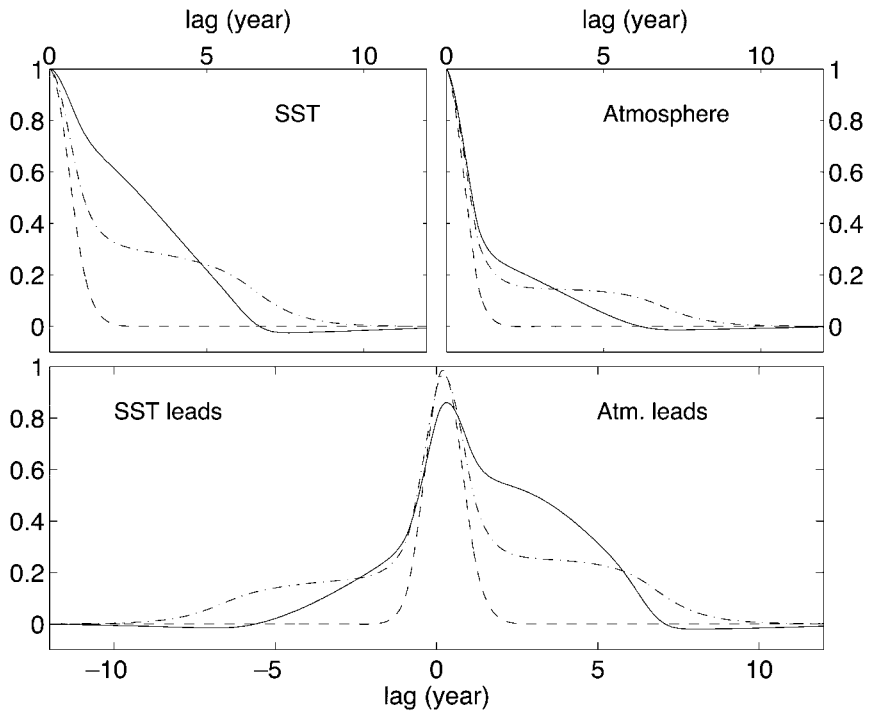

FIG. 14. (top) Autocorrelation of yearly averaged SST and air temperature and (bottom) cross correlation between the two variables at $x = -4000$ km for the entrainment case with $\lambda_y = 5400$ km (solid line) and $\lambda_y = 5600$ km (dashed–dotted line). Reference for the uncoupled case is given for $\lambda_y = 5400$ km (dashed line).

limited predictability of the one-dimensional model of Bretherton and Battisti (2000).

1) COUPLING BY ENTRAINMENT

Figure 10 (right) compares the autocorrelation function of ψ_o at $x = -4000$ km in the passive and coupled cases. In both cases, the persistence is large and the autocorrelations much smoother than the power spectra. This occurs because the phase relations between the free and forced oceanic response that caused its peaks and throughs corresponded to specific frequencies whereas the autocorrelation is an integral over all frequencies. Since coupling by entrainment primarily increases the power of ψ_o at periods longer than a decade but does not significantly alter the spectral shape, it changes little the geostrophic persistence. However, the geostrophic fluctuations strongly alter the autocorrelation function of SST. Figure 14 (solid and dashed–dotted lines) clearly shows the two SST timescales in the coupled case; a short timescale that corresponds to that of the oceanic mixed layer, and a longer one that reflects the geostrophic modulation. Like the power spectrum, the autocorrelation function is sensitive to l and the long-term persistence is maximum in near-barotropic conditions. Although the correlation levels are lower and the sensitivity to l smaller, the two timescales also appear in the autocorrelation of $\tilde{\psi}$. In both cases, the long-term persistence increases with the distance from the eastern boundary, because of the zonal dependence of the geostrophic fluctuations.

As seen in the cross correlation between $\tilde{\psi}$ and SST (Fig. 14, bottom), the long geostrophic timescale enhance the atmospheric predictability since there is a small but persistence correlation when SST preceeds the atmosphere by as much as 5–8 yr, depending on l. Using the square of the lagged correlation as a coarse measure of predictive skill (the fraction of variance that can be predicted), about 2% (depending on λ_y) of the yearly climatic variability could thus be predicted from yearly SST data several years before. Such predictive skill is very small, but it increases for averages over a longer duration (averaging reduces the unpredictable short timescale variability). For instance, the predictive skill at 5-yr lead reaches 4% using 3-yr averages and ranges from 1% to 9% using 5-yr averages for λ_y between 5600 and 5400 km. In most cases, $\tilde{\psi}$ can be equally well predicted from earlier values of $\tilde{\psi}$ or SST, while predictions based on ψ_o are inferior (see below). However, in practice, $\tilde{\psi}$ is likely to be obscured by other sources of variability. Since improved predictive skill could be obtained from more sophisticated forecast models, they may be of some practical value. This demonstrates that Bretherton and Battisti's (2000) conclusion that true NAO predictability is limited to 6 months or so is a direct consequence of the simplicity of their ocean mod-

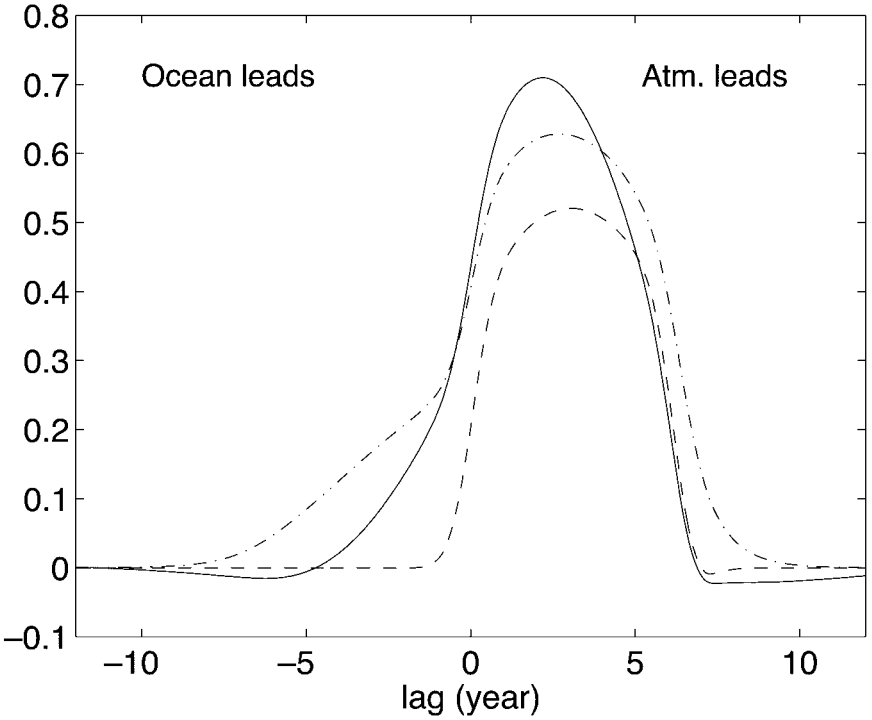

FIG. 15. Cross correlation between yearly averaged air temperature and ψ_o at $x = -4000$ km for the entrainment case for $\lambda_y = 5400$ km (solid line) and $\lambda_y = 5600$ km (dashed–dotted line). Reference for the uncoupled case is given for $\lambda_y = 5400$ km (dashed line).

el, which neglects the geostrophic variability of the ocean interior.

The cross correlation between ψ_o and $\tilde{\psi}$ is given in Fig. 15. In the passive case (dashed line), it has a broad peak when ψ_o lags $\tilde{\psi}$ by a few years and is negligible when it leads. The adjustment time at $x = -4000$ km is about 3.1 yr, which is approximately the Rossby wave transit time from the center of action of the wind stress (see Jin 1997). In the coupled case, the cross correlation still primarily reflects the wind stress forcing of the ocean interior, but there now is a small predictability when the ocean leads. Also, the delay between the wind stress forcing and ψ_o is shorter (2.2 yr for $\lambda_y = 5400$ km and 2.7 yr for $\lambda_y = 5600$ km), consistent with the increase in phase speed (Fig. 6). This can be compared to the short delay found between the NAO and the changes in the Gulf Stream path, if the latter reflect an adjustment to the changes in Sverdrup transport. Using observations, Taylor and Stephens (1998) found a 2-yr lag while Frankignoul et al. (2001) found a 1–1.5-yr lag, and Halliwell (1998) obtained a 2-yr lag in a simulation with an oceanic GCM.

The entrainment case bears resemblance with the coupled ocean–atmosphere mode seen in the ECHAM1/LSG coupled GCM (Frankignoul et al. 2000). As shown in Fig. 16, the mostly second dominant mode of a maximum covariance analysis based on a singular value decomposition (SVD) between the baroclinic pressure at 250 m and the sea level pressure has similar patterns to those described in Fig. 5. When the atmosphere leads, the thermocline motions reflect the oceanic response to the wind stress forcing. When the ocean leads, a depressed thermocline is associated with a warm SST anomaly and a downstream sea level pressure high (see also their Fig. 8). As in the present model, there is little change of patterns between lead and lag conditions and the antisymetric distribution with lag of the covariance is broadly consistent with that seen between $\tilde{\psi}$ and ψ_o in Fig. 15. A positive ocean–atmosphere feedback similar to that investigated here may thus be at play in the coupled model. Note that is the GCM case, the maximum correlation between ψ_o and the atmosphere is found when the latter leads by 1 yr, which is shorter than in Fig. 15. However, the 1-yr delay pertains to basinwide patterns and is indeed expected to be much shorter than at 4000 km from the eastern boundary.

The zonal distribution of the variance in the coupled case is shown in Fig. 11 (solid line) for yearly (thin) and 5-yr (thick) averages. Coupling with the ocean interior results in a strong westward intensification of the SST variance but, as mentioned above, this is mostly due is due to the geostrophic modulation, not to the active coupling whose influence is that seen for ψ_o. The atmospheric variance increases only slightly in the central and western part of the basin. It is thus primarily determined by the uncoupled dynamics of the atmosphere, in agreement with GCM experiments (e.g., Saravanan 1998). Note that the 5-yr averaging has little

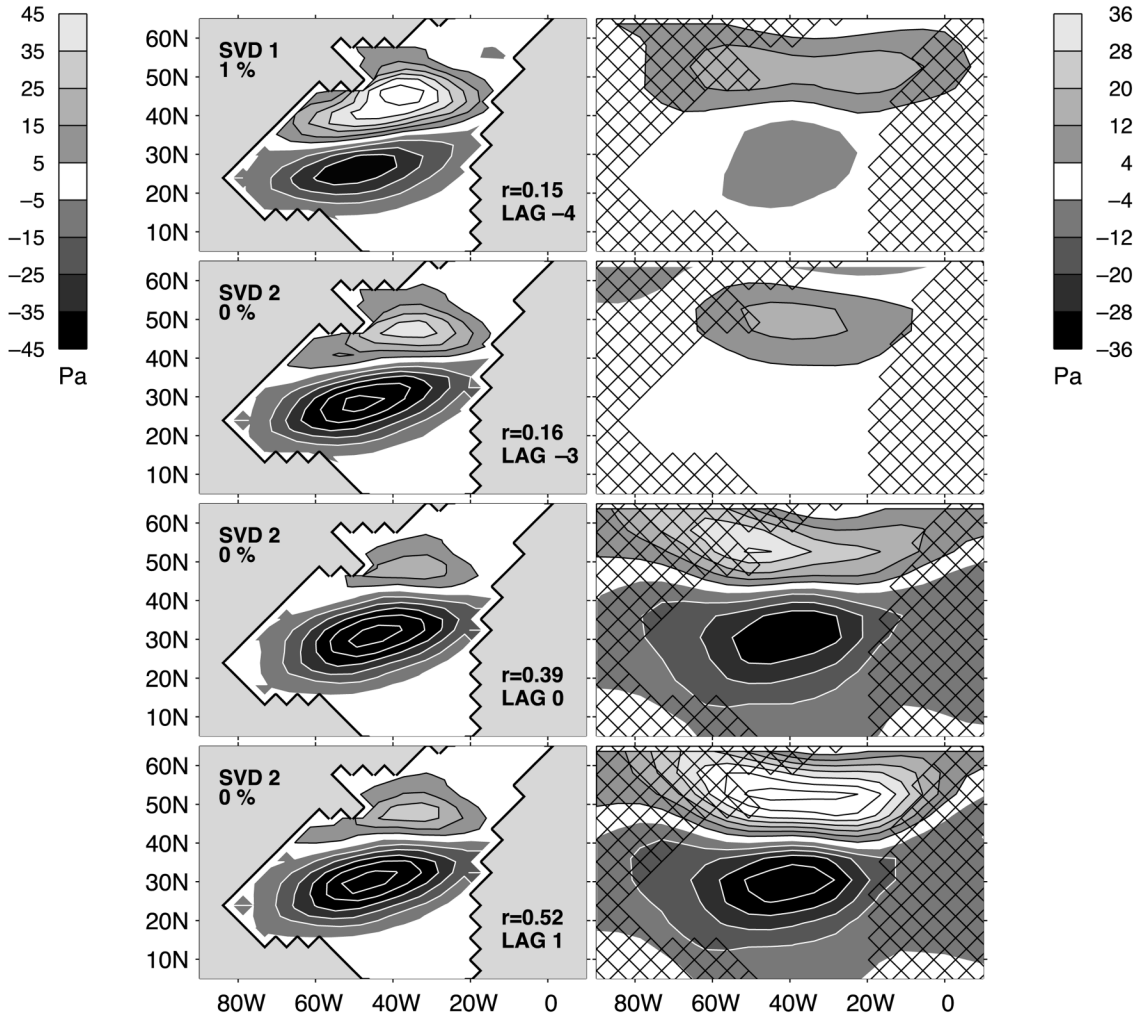

FIG. 16. Maps for (left) the baroclinic pressure at 250 m in the ocean (Pa) and (right) the sea level pressure (Pa) for the (mostly) second dominant SVD mode at significant lags between −4 and 1 (positive when the atmosphere leads) when their (upper-left side) significance level is below 5%. The SVD times series are normalized so that the maps indicate typical amplitudes. Positive (negative) isolines are in black (white). Lag, mode number, and correlation are also indicated (after Frankignoul et al. 2000).

influence on ψ_o, which is dominated by long timescales, but significantly reduces the SST and $\tilde{\psi}$ variance.

2) COUPLING BY SST ADVECTION

As discussed above, coupling by advection only significantly enhances the geostrophic response in near-resonant conditions, and the enhancement increases with frequency. Since the power density of ψ_o strongly decreases at periods shorter than 10 yr, the impact of the positive wind stress feedback is strongest at a period of about 12 yr, resulting in a slightly oscillatory behavior. Thus, the autocorrelation function of ψ_o changes sign and has a small minimum at a lag of half this period (Fig. 13). Because of the strong imprint of geostrophic fluctuations on SST, the oscillatory behavior also appears in the autocorrelation and in the cross correlation of SST and $\tilde{\psi}$ (Fig. 17), reflecting the enhanced decadal variability seen in Fig. 12. Note that we have only considered 5-yr averages in Fig. 17, to remove some of the influence of the periods which are ill represented by our model. Several observational studies have reported an oscillatory behavior at decadal periods for SST and sea level pressure in the North Atlantic (e.g., Deser and Blackmon 1993) and subsurface temperature (Molinari et al. 1997) in the North Atlantic. The present study suggests that it might be linked to ocean–atmosphere coupling and SST advection by the wind-driven geostrophic motions.

7. Conclusions

Using a two-layer quasigeostrophic channel atmosphere, we have studied the coupling between geostrophic motions in the ocean and the natural variability of the atmosphere at the decadal timescale, and we have

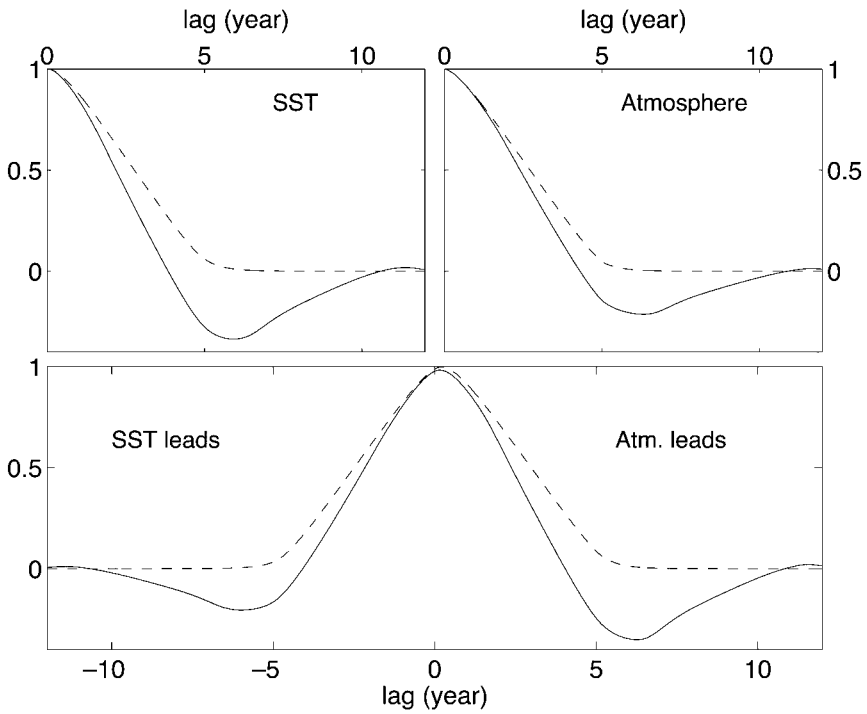

FIG. 17. (top) Autocorrelation of 5-yr-averaged SST and air temperature and (bottom) cross correlation between the two variables at $x = -4000$ km for the advection case with $\lambda_y = 5600$ km (solid line). Reference for the uncoupled case is given in dashed line.

established the statistical signatures of the interaction. To set the stage for the analysis, we first considered the coupling between the atmosphere and the oceanic mixed layer, thus extending the work of Barsugli and Battisti (1998) and Saravanan and McWilliams (1998) to the case of a dynamical atmosphere. This has allowed us to investigate the wavenumber dependence of the SST adjustment to air temperature change that is found at low frequency showing that there is an increase in power enhancement with increasing zonal scale, as seen in GCM experiments (Bladé 1997; Manabe and Stouffer 1996).

The coupling with the ocean interior occurs via entrainment and meridional advection. In both cases, a positive feedback may occur between the ocean interior and the atmosphere, leading to Rossby-like coupled modes that grow as they propagate westward. In the entrainment case, the vertical displacement of isopycnals generate subsurface temperature anomalies that result in SST anomalies and, through surface heat exchanges, air temperature anomalies of the same sign. Positive feedback only occurs for equivalent barotropic conditions because they are needed for the wind stress to reinforce the original geostrophic fluctuations. Then, the atmospheric pressure is nearly in phase with the SST perturbation that is itself only slightly downstream of the thermocline depth perturbation, and the positive wind stress feedback can overcome the negative heat flux one. Since coupling by entrainment is most efficient at low frequency, it is well represented in our simplified model, yielding a small power enhancement of the ψ_o spectrum for decadal and longer periods. The coupling also decreases the apparent delay between the interior response and the wind stress forcing. In our standard wintertime conditions, the range of unstable meridional wavelength is between 5200 and 5800 km, but larger meridional scales could have been obtained for stronger mean winds. For instance, taking $U_1 = 21$ m s^{-1} and $U_2 = 10$ m s^{-1} as representative of extreme wintertime conditions, the range of unstability is between 5800 and 6400 km. These scales are roughly consistent with that of NAO, suggesting that the latter may well be sustained at low frequency by the coupling with the geostrophic variability in the ocean interior. However, as entrainment is not effective in summer, the instability is intermittent, and the predicted growth rates somewhat overestimated. Note that, although the spatial structure of the stochastic forcing would need to be adapted, the model should also be applicable to the North Pacific, yielding larger amplitudes and longer dominant periods as the basin is larger.

The geostrophic modulation by entrainment significantly affects the SST and air temperature spectra at periods longer than about 10 yr, slightly reddening the predicted atmospheric spectrum down to periods of 20 or 30 yr. Such reddening is found in the observed NAO spectrum (Hurrel and van Loon 1997; Wunsch 1999). Coupling by entrainment does not result in a quasi-

oscillatory behavior but it yields a significant correlation between SST and the atmosphere when the former leads the latter by a few years. Using 5-yr average, the predictive skill in our model is significant, reaching up to 9% 5 yr in advance. The overall influence of the coupling on the atmosphere is nonetheless weak and the spatial pattern remains determined by uncoupled atmospheric dynamics. The statistical signatures of the interaction suggest that this mechanism may be at play in the ECHAM1/LSG coupled model where a weak positive ocean–atmosphere feedback was detected (Frankignoul et al. 2000). Indeed, the oceanic and atmospheric perturbations of the coupled model were approximately in phase, and there was no change of sign between lead and lag conditions in the cross-correlation function between ψ_o (or SST) and $\tilde{\psi}$. Whether coupling by entrainment is also prevalent with a less diffusive ocean model remains to be established.

In the SST advection case, geostrophic advection of warm water from the south, say, generates a positive SST anomaly and then a positive air temperature anomaly. Provided the atmospheric response to the SST is equivalent barotropic and shifted downstream, the surface wind stress reinforces the northward meridional velocity, hence acting as a positive feedback. The efficiency of the mechanism increases with frequency and is maximum on timescales of a few years. Unfortunately, the latter are not well represented in our model where the zonal scale was assumed to be much larger than the meridional one, and further investigations are needed. In any case, coupling by SST advection introduces a small oscillatory behavior at the decadal timescale, as observed in the North Atlantic. This is also predicted by the scenario of Latif and Barnett (1994). However, the present model differs from the latter since the heat flux feedback is negative, not positive, and the air–sea coupling takes place over the whole basin, albeit with stronger effects as one moves westward, and not via the western boundary current fluctuations.

The simplicity of our coupled model should be emphasized. Its main weakness for the atmosphere is a crude vertical resolution, the lack of mean horizontal shear, and the neglect of the synoptic variability. As shown by Palmer and Sun (1985) and others, transients and the changes of the storm track play an active role in setting the low-frequency response of the atmosphere to SST anomalies, hence they may strongly influence the nature of the ocean–atmosphere coupling. The ocean is also oversimplified, in particular as we have neglected western boundary dynamics, although the western boundary currents and their associated meridional heat transport play a key role in several mechanisms of decadal variability (Latif and Barnett 1994; Cessi 2000; Marshall et al. 2001). Although the robustness of our analysis needs to be addressed in a more realistic model, the present results seem nonetheless relevant to the air–sea coupling over most of the midlatitude ocean basins.

Acknowledgments. This research was supported in part by a grant from the PNEDC and Grant ENV4-CT98-0714 of the European Community (SINTEX). David Ferreira was supported by a bursary from the DGA-CNRS and John Marshall received support from NOAA's Office of Global Programs.

APPENDIX A

Derivation of the Coupled Model

Here we derive the coupled model whose properties are studied in the body of the paper.

a. Atmosphere

The atmospheric fluctuations are assumed to be in equilibrium with the ocean and governed by the linear quasigeostrophic vorticity and thermodynamic equations in a β plane:

$$U_a \frac{\partial}{\partial x}\nabla^2\psi_a + \beta\frac{\partial}{\partial x}\psi_a = f\frac{\partial}{\partial z}w_a \tag{A1}$$

$$U_a \frac{\partial}{\partial x}\theta + \upsilon_a\frac{\partial\overline{\theta}}{\partial y} + w_a\frac{\partial\overline{\theta}}{\partial z} = \frac{q}{C_{pa}} - \gamma_r\theta, \tag{A2}$$

where $U_a(z)$ is the mean zonal wind (only function of the vertical coordinate), w_a and υ_a are the vertical and meridional velocity, θ is the potential temperature, f is the Coriolis parameter, β is its meridional gradient, γ_r represents radiative and other damping, q is the diabatic heating per unit mass, and C_{pa} is the air heat capacity. The vorticity equation (A1) is evaluated at the upper and lower levels of a two-level atmosphere, and the thermodynamic Eq. (A2) evaluated at midlevel (see Fig. 2). Defining barotropic and baroclinic components:

$$(\hat{\cdot}) = (\cdot)_1 + (\cdot)_2, \qquad (\tilde{\cdot}) = (\cdot)_1 - (\cdot)_2, \tag{A3}$$

equations for the evolution of barotropic and baroclinic potential vorticity can be written—see Eqs. (24) and (25) of GM:

$$\hat{U}\partial_x\nabla^2\hat{\psi} + \hat{\beta}\partial_x\hat{\psi} + \tilde{U}\partial_x\nabla^2\tilde{\psi} = 0 \tag{A4}$$

$$\tilde{U}\partial_x\nabla^2\hat{\psi} + \tilde{\beta}\partial_x\hat{\psi} + \hat{U}\partial_x\left(\nabla^2\tilde{\psi} - \frac{2}{L_a^2}\tilde{\psi}\right) + \hat{\beta}\partial_x\tilde{\psi}$$

$$= \frac{4}{L_a^2}\left(\gamma_{Ta}\tilde{\psi} - \frac{\gamma_a}{r_a}T\right) + F_s \tag{A5}$$

with $\hat{\beta} = 2\beta$, $\beta = 2\tilde{U}/L_a^2$, $\gamma_a = \lambda/\rho_a C_{pa} H_a$, and $\gamma_{T_a} = \gamma_a + \gamma_r$. In (A5), a white noise stochastic forcing F_s has been included to represent stirring by baroclinic instability and other nonrepresented dynamics. Also, θ has been converted to $\tilde{\psi}$ using the thermal wind relation thus

$$\theta = \frac{2f\theta_a}{gH_a}\tilde{\psi} = r_a\tilde{\psi}, \tag{A6}$$

where θ_a is a typical atmospheric temperature and H_a the depth of the troposphere. The surface heat flux Q has been set proportional to the air–sea temperature difference, so that

$$q = \frac{Q}{\rho_a C_{pa} H_a} = \frac{\lambda}{\rho_a C_{pa} H_a}(T - \theta), \tag{A7}$$

where T is the SST anomaly, λ is the heat exchange coefficient, and ρ_a is the air density.

We are mostly interested in large-scale, low-frequency midlatitudes fluctuations. Since such fluctuations in the atmosphere have patterns with a zonal scale much larger than the meridional one, we suppose that

$$\nabla^2 \sim \partial_y^2 = -l^2, \tag{A8}$$

where l is meridional wavenumber. Although this approximation is somewhat limiting, as discussed below, it simplifies considerably the algebra and allows (A4) to be written thus

$$\hat{\psi} = -\mu\tilde{\psi} \tag{A9}$$

with

$$\mu = \frac{\tilde{U}}{\hat{U} - \dfrac{\hat{\beta}}{l^2}}. \tag{A10}$$

The relative strength of the barotropic and baroclinic modes is controlled entirely by μ. On scales close to that of stationary barotropic Rossby waves $l = \sqrt{\hat{\beta}/\hat{U}}$ ($=2\pi/5236$ km^{-1} for our standard values), $|\mu|$ is very large and atmospheric perturbations are nearly barotropic. When μ is large and negative ($\mu < -2$ for our choice below of extrapolation to the surface), the fluctuations are equivalent barotropic. For μ large and positive, they also keep the same sign, but the amplitude decreases with height. When $|\mu|$ is small, the perturbations change sign in the vertical: in the long-wave limit ($l^2 \ll \hat{\beta}/\hat{U}$), they are highly baroclinic ($\psi_1 \sim -\psi_2$) while in the short-wave limit ($l^2 \gg \hat{\beta}/\hat{U}$) the perturbation is larger in the lower layer, the ratio ψ_1/ψ_2 being scaled by $-U_2/U_1$ (or $\tilde{\psi}/\hat{\psi}$ by $-\tilde{U}/\hat{U}$).

Rearranging (A5) it can be written:

$$(\Gamma_T + V\partial_x)\theta = \Gamma_a T + F \tag{A11}$$

with

$$\Gamma_{a,r} = \frac{4\gamma_{a,r}}{l^2 L_a^2}, \tag{A12}$$

$$\Gamma_T = \Gamma_a + \Gamma_r, \tag{A13}$$

where Γ_a and Γ_r are the (inverse) thermal and radiative timescale of the potential vorticity anomaly and

$$V = -\tilde{U}\mu + \frac{\tilde{\beta}}{l^2}\mu + \frac{\hat{U}}{l^2}\left(l^2 + \frac{2}{L_a^2}\right) - \frac{\hat{\beta}}{l^2} \tag{A14}$$

represents atmospheric dynamics and is a measure of the Doppler-shifted phase speed of a free Rossby wave in the atmosphere.

Over land ($x > 0$), we set $\gamma_a = 0$ in (A5): land is assumed to have a negligible heat capacity so that its temperature is always adjusted to that of the atmosphere and there are no anomalies in diabatic heating.

The surface streamfunction is linearly extrapolated from uppers levels:

$$\psi_s = \frac{1}{2}\hat{\psi} - \tilde{\psi} = -\left(1 + \frac{\mu}{2}\right)\frac{\theta}{r_a} = -m\theta. \tag{A15}$$

For simplicity, we neglect the effect of surface friction on atmospheric perturbations.

b. Sea surface temperature

The ocean is topped by a slab mixed layer of constant depth h_{mix}. Assuming a mean meridional SST gradient $\partial\overline{T}/\partial y$, we represent the evolution of the mixed layer temperature anomalies T by

$$\frac{\partial T}{\partial t} + v_o\frac{\partial \overline{T}}{\partial y} = \gamma_e(T_o - T) - \frac{Q}{\rho_o C_{po} h_{\text{mix}}}, \tag{A16}$$

where v_o is the meridional surface geostrophic velocity, T_o is the temperature anomaly below the mixed layer, Q is the surface heat flux as defined in (A7), C_{po} is the water heat capacity, ρ_o is the water density, and γ_e parameterizes entrainment and vertical mixing. For simplicity, we have neglected effects such as Ekman advection, horizontal mixing, and mixed layer depth variation, and so the above leads to an overestimate of the role of the surface heat exchanges in generating the SST anomalies. Following GM, we assume that the thermal anomalies being entrained reflect the adiabatic undulation of the isopycnal surfaces underlying the mixed layer, and so can be related to vertical displacements $\zeta = \psi_o(x, y, t)Z(z)$, where Z is the vertical profile of the first mode displacement. Then, the subsurface temperature anomaly can be expressed in term of the baroclinic streamfunction by

$$T_o = -\frac{\partial \overline{T}_o}{\partial z}\zeta = -\frac{\partial \overline{T}_o}{\partial z}Z(h_{\text{mix}})\psi_o = r_o\psi_o, \tag{A17}$$

where $\partial\overline{T}_o/\partial z$ is the temperature gradient below the mixed layer. Similarly, the geostrophic advection term in (A16) can be expressed in term of ψ_o by

$$v_o\frac{\partial \overline{T}}{\partial y} = \frac{\partial \overline{T}}{\partial y}\phi(0)\frac{\partial \psi_o}{\partial x} = -ar_o\frac{\partial \psi_o}{\partial x}, \tag{A18}$$

where $ar_o = -\phi(0)\partial\overline{T}/\partial y$.

Then, (A16) becomes

$$\frac{\partial T}{\partial t} = \gamma_e(r_o\psi_o - T) + \gamma_s(\theta - T) + ar_o\frac{\partial \psi_o}{\partial x} \tag{A19}$$

with $\gamma_s = \lambda/\rho_o C_{po} h_{\text{mix}}$.

c. Ocean interior

We consider a semi-infinite ocean bounded to the east by land for $x > 0$ (Fig. 2). Oceanic western boundary dynamics are not represented and our calculation is limited to $x > -L$. The ocean is linearized about a state of rest and obeys quasigeostrophic β-plane dynamics. As shown in FMZ the barotropic mode can be neglected at low frequencies, and so our ocean interior is represented by a first baroclinic mode forced by stochastic Ekman pumping. The geostrophic streamfunction is given by $\psi_o(x, y, t)\phi(z)$ where the first mode vertical profile $\phi(z)$ is normalized by $\int_{-H_o}^{0} \phi(z)^2\, dz = H_o$. In the long-wave approximation, it evolves according to

$$\partial_t \frac{\psi_o}{c_o} + \partial_x \psi_o = \frac{\phi(0)}{\rho_o H_o \beta} \nabla \times \tau, \tag{A20}$$

where c_o is the speed of the first baroclinic Rossby wave, τ is the surface wind stress, and H_o is the constant depth of the ocean. We impose a radiation condition in the west and a no-normal flow condition at the eastern boundary:

$$\psi_o = 0 \quad \text{at } x = 0. \tag{A21}$$

Over the ocean we assume that the surface wind stress perturbation is proportional to the surface wind:

$$\frac{\phi(0)}{\rho_o H_o} \nabla \times \tau = \alpha' \nabla^2 \psi_s, \tag{A22}$$

so that, (A20) becomes

$$\partial_t \frac{\psi_o}{c_o} + \partial_x \psi_o = -\alpha \psi_s \tag{A23}$$

with

$$\alpha = \frac{\alpha' l^2}{\beta}. \tag{A24}$$

d. Numerical parameters

Standard values for the parameters are chosen to be representative of winter parameters (Table 1), but note that some of them differ from those of GM. Our choice for the atmosphere is traditional, using 35°–40°N as reference latitudes and a rather strong radiative damping $\gamma_r \sim (8 \text{ days})^{-1}$, to make up for the neglect of surface friction. The heat exchange coefficient γ_a is derived using $\lambda = 40 \text{ W m}^{-2} \text{ K}^{-1}$. An atmospheric heat capacity of $10^7 \text{ J m}^{-2} \text{ K}^{-1}$ implies $\gamma_a^{-1} \sim 3$ days. The oceanic ''entrainment'' feedback $\gamma_e \sim (1 \text{ yr})^{-1}$ may seem weak but is broadly consistent with the observed persistence of midlatitude sea surface salinity anomalies (Hall and Manabe 1997), which are not directly affected by the heat flux feedback and thus provide a direct estimate of its averaged strength. The heat flux damping factor γ_s was derived using a mixed layer depth $h_{\text{mix}} = 100$ m. In the absence of air temperature adjustment, the SST anomaly damping timescale due to heat flux is thus about four months. Choosing a typical temperature of 290 K for a 10-km height troposphere gives $r_a = 4.5 \times 10^{-7} \text{ K s m}^{-2}$. To estimate r_o and a, we use $\phi(0) = 3$ and $Z(100) = -1.5 \times 10^{-2} \text{ s m}^{-1}$, from Richman et al. (1977), so that for $\partial_z \overline{T}_o = 1.2 \times 10^{-2}$°C m^{-1} and $\partial_y \overline{T} = -5 \times 10^{-6}$°C m^{-1} we find $r_o = 2 \times 10^{-4}$ K s m^{-2} and $a = 7.5 \times 10^{-2} \text{ m s}^{-1}$. Last, as in GM, we relate the wind stress anomaly to the surface wind speed anomaly by linearizing the bulk drag law about the mean surface value u_s:

$$\tau = 2\rho_a C_D \overline{u}_s u_s. \tag{A25}$$

Comparing (A22) and (A25), we obtain

$$\alpha' = 2\rho_a C_D \overline{u}_s \frac{\phi(0)}{\rho_o H_o}. \tag{A26}$$

Using $C_D = 1.5 \times 10^{-3}$ and $\overline{u}_s = 5 \text{ m s}^{-1}$, we find $\alpha' = 1.3 \times 10^{-8} \text{ s}^{-1}$.

APPENDIX B

The Weak Coupling Case

If the coupling is weak enough, that is, the SST modulation by the ocean interior entails a small perturbation of the free modes, one can derive simple expressions for the roots of (14):

$$\delta_1 \simeq ik_o + \frac{c\Gamma}{2V}\left(a + \frac{M}{ik_o + \dfrac{\Gamma}{V}}\right) \tag{B1}$$

$$\delta_2 \simeq -\frac{\Gamma}{V} - \frac{c\Gamma}{2V}\left(a - \frac{M}{ik_o + \dfrac{\Gamma}{V}}\right) \tag{B2}$$

with

$$M = 2\gamma_e + a\left(ik_o - \frac{\Gamma}{V}\right) + \frac{ca^2}{2}\frac{\Gamma}{V}.$$

When the SST modulation occurs by entrainment and the influence of geostrophic advection is neglected, taking $a = 0$, (B1) simplifies to

$$\delta_1 = ik_o + \frac{c\gamma_e}{1 + i\dfrac{Vk_o}{\Gamma}}$$

$$= ik_o + \frac{\alpha r_o}{r_a}\frac{\Gamma_a}{\Gamma}\frac{\gamma_e}{(\gamma_{To} - i\omega)}\frac{1 + \dfrac{\mu}{2}}{\left(1 + i\dfrac{Vk_o}{\Gamma}\right)}. \tag{B3}$$

The mode is a westward-propagating oceanic Rossby wave whose wavelength has been modified by the coupling (imaginary part of the second term). It grows (decays) as it propagates when the real part of δ_1 is negative

(positive). The zonal wavenumber of the free mode, given by the imaginary part of δ_1, is

$$\mathrm{Im}(\delta_1) = k_o\left[1 - \frac{\alpha r_o}{r_a}\frac{\Gamma_a}{\Gamma}\frac{\gamma_e}{\gamma_{To}}\frac{\left(1 + \frac{\mu}{2}\right)}{1 + \left(\frac{Vk_o}{\Gamma}\right)^2}\frac{V}{\Gamma}\right]. \quad \text{(B4)}$$

When the SST modulation occurs by geostrophic advection and the influence of entrainment is neglected, (B1) becomes

$$\delta_1 = ik_o + \frac{ik_oca + \left(\frac{ca}{2}\right)^2\frac{\Gamma}{V}}{1 + i\frac{k_oV}{\Gamma}} \quad \text{(B5)}$$

or, to first order in a:

$$\delta_1 = ik_o + \frac{ik_oca}{1 + i\frac{k_oV}{\Gamma}}$$

$$= ik_o + \frac{\alpha r_o}{r_a}\frac{\Gamma_a}{\Gamma}\frac{ik_oa}{\gamma_{To} - i\omega}\frac{1 + \frac{\mu}{2}}{1 + i\frac{Vk_o}{\Gamma}}, \quad \text{(B6)}$$

which is the equivalent of (B3) but with ik_oa instead of γ_e. The mode is also an oceanic Rossby wave that grows or decays as it propagates westward, but here the strength of the coupling primarily depends on $v_o = \partial_x\psi_o$ and hence on k_o, so that the growth rate is expected to increase with frequency. From (B5), the zonal wavenumber is

$$\mathrm{Im}(\delta_1) = k_o\left[1 + \frac{\alpha r_o}{r_a}\frac{\Gamma_a}{\Gamma}\frac{a}{\gamma_{To}}\frac{1 + \frac{\mu}{2}}{1 + \left(\frac{Vk_o}{\Gamma}\right)^2}\right]. \quad \text{(B7)}$$

REFERENCES

Alexander, M. A., and C. Deser, 1995: A mechanism for the recurrence of wintertime midlatitude SST anomalies. *J. Phys. Oceanogr.*, **25,** 122–137.

——, and C. Penland, 1997: Variability of a mixed layer ocean model driven by stochastic atmospheric forcing. *J. Climate*, **10,** 2424–2442.

Barsugli, J. J., and D. S. Battisti, 1998: The basic effects of atmosphere–ocean thermal coupling on midlatitude variability. *J. Atmos. Sci.*, **55,** 477–493.

Bladé, I., 1997: The influence of the midlatitude ocean/atmosphere coupling on the low-frequency variability of a GCM. Part I: No tropical SST forcing. *J. Climate*, **10,** 2087–2106.

Bretherton, C. S., and D. S. Battisti, 2000: An interpretation of the results from atmospheric general circulation models forced by the time history of the observed sea surface temperature distribution. *Geophys. Res. Lett.*, **27,** 767–770.

Cessi, P., 2000: Thermal feedback on the wind stress as a contributing cause of climate variability. *J. Climate*, **13,** 232–244.

Czaja, A., and C. Frankignoul, 1999: Influence of the North Atlantic SST on the atmospheric circulation. *Geophys. Res. Lett.*, **26,** 2969–2972.

Delworth, T. L., 1996: North Atlantic variability in a coupled ocean–atmosphere model. *J. Climate*, **9,** 2356–2375.

Deser, C., and M. L. Blackmon, 1993: Surface climate variations over the North Atlantic Ocean during winter 1900–1989. *J. Climate*, **6,** 1743–1753.

Egger, J., 1977: On the linear theory of the atmospheric response to sea surface temperature anomalies. *J. Atmos. Sci.*, **34,** 603–614.

Ferranti, L., F. Molteni, and T. N. Palmer, 1994: Impact of localized tropical and extratropical SST anomalies in ensembles of seasonal GCM integrations. *Quart. J. Roy. Meteor. Soc.*, **120,** 1613–1645.

Frankignoul, C., 1985: Sea surface temperature anomalies, planetary waves and air–sea feedback in the middle latitudes. *Rev. Geophys.*, **23,** 357–390.

——, 1999: A cautionary note on the use of statistical atmospheric models in the middle latitudes: Comments on ''Decadal variability in the North Pacific as simulated by a hybrid coupled model.'' *J. Climate*, **12,** 1871–1872.

——, and K. Hasselmann, 1977: Stochastic climate models. Part II: Application to sea-surface temperature anomalies and thermocline variability. *Tellus*, **29,** 284–305.

——, P. Müller, and E. Zorita, 1997: A simple model of the decadal response of the ocean to stochastic wind forcing. *J. Phys. Oceanogr.*, **27,** 1533–1546.

——, A. Czaja, and B. L'Heveder, 1998: Air–sea interaction in the North Atlantic and surface boundary conditions for ocean models. *J. Climate*, **11,** 2310–2324.

——, E. Kestenare, N. Sennéchael, G. de Coëtlogon, and F. D'Andrea, 2000: On decadal-scale ocean–atmosphere interactions in the extended ECHAM1/LSG climate simulation. *Climate Dyn.*, **16,** 333–354.

——, G. de Coëtlogon, T. M. Joyce, and S. Dong, 2001: Gulf Stream variability and ocean–atmosphere interactions. *J. Phys. Oceanogr.*, in press.

Goodman, J., and J. Marshall, 1999: A model of decadal middle-latitude atmosphere–ocean coupled modes. *J. Climate*, **12,** 621–641.

Grötzner, A., M. Latif, and T. P. Barnett, 1998: A decadal climate cycle in the North Atlantic Ocean as simulated by the ECHO coupled GCM. *J. Climate*, **11,** 831–847.

Hall, A., and S. Manabe, 1997: Can local linear stochastic theory explain sea surface temperature and salinity variability? *Climate Dyn.*, **13,** 176–180.

Halliwell, G. R., Jr., 1998: Simulation of North Atlantic decadal/multidecadal winter SST anomalies driven by basin-scale atmospheric circulation anomalies. *J. Phys. Oceanogr.*, **28,** 5–21.

——, and D. A. Mayer, 1996: Frequency response properties of the forced climatic SST anomaly variability in the North Atlantic. *J. Climate*, **9,** 3575–3587.

Held, I. M., 1983: Stationary and quasi-stationary eddies in the extratropical troposphere: Theory. *Large Scale Dynamical Processes in the Atmosphere*, R. P. Pearce and B. J. Hoskins, Eds., Academic Press, 127–168.

Hurrel, J. W., and H. van Loon, 1997: Decadal variations in climate associated with the North Atlantic oscillation. *Climatic Change*, **36,** 301–326.

Jin, F.-F., 1997: A theory of interdecadal climate variability of the North Pacific ocean–atmosphere system. *J. Climate*, **10,** 1821–1835.

Kushnir, Y., and I. M. Held, 1996: Equilibrium atmospheric response to North Atlantic SST anomalies. *J. Climate*, **9,** 1208–1220.

Latif, M., and T. P. Barnett, 1994: Causes of decadal climate variability in the North Pacific/North American sector. *Science*, **266,** 634–637.

Manabe, S., and R. J. Stouffer, 1996: Low-frequency variability of surface air temperature in a 1000-year integration of a coupled atmosphere–ocean–land surface model. *J. Climate,* **9,** 376–393.

Marshall, J., and D. K. So, 1990: Thermal equilibration of planetary waves. *J. Atmos. Sci.,* **47,** 963–978.

——, H. L. Johnson, and J. Goodman, 2001: A study of the interaction of the North Atlantic oscillation with ocean circulation. *J. Climate,* **14,** 1399–1421.

Molinari, R. L., D. A. Mayer, J. F. Festa, and H. F. Bezdek, 1997: Multiyear variability in the near-surface temperature structure of the midlatitude western North Atlantic. *J. Geophys. Res.,* **102,** 3267–3278.

Neelin, J. D., and W. Weng, 1999: Analytical prototypes for ocean–atmosphere interaction at midlatitudes. Part I: Coupled feedbacks as a sea surface temperature dependent stochastic process. *J. Climate,* **12,** 697–721.

Palmer, T. N., and Z. Sun, 1985: A modelling and observational study of the relationship between sea surface temperature in the northwest Atlantic and the atmospheric general circulation. *Quart. J. Roy. Meteor. Soc.,* **111,** 947–975.

Peng, S., L. A. Mysak, H. Richie, J. Derome, and B. Dugas, 1995: The differences between early and midwinter atmospheric responses to sea surface temperature anomalies in the northwest Atlantic. *J. Climate,* **8,** 137–157.

Richman, J. G., C. Wunsch, and N. G. Hogg, 1977: Space and time scales of mesoscale motion in the Western North Atlantic. *Rev. Geophys. Space Phys.,* **15,** 385–420.

Rodwell, M. J., D. P. Rowell, and C. K. Folland, 1999: Oceanic forcing of the wintertime North Atlantic oscillation and European climate. *Nature,* **398,** 320–323.

Saravanan, R., 1998: Atmospheric low-frequency variability and its relationship to midlatitude SST variability: Studies using the NCAR Climate System model. *J. Climate,* **11,** 1386–1404.

——, and J. C. McWilliams, 1998: Advective ocean–atmosphere interaction: An analytical stochastic model with implications for decadal variability. *J. Climate,* **11,** 165–188.

Shutts, G., 1987: Some comments on the concept of thermal forcing. *Quart. J. Roy. Meteor. Soc.,* **113,** 1387–1394.

Sirven, J., and C. Frankignoul, 2000: Variability of the thermocline due to a sudden change in the Ekman pumping. *J. Phys. Oceanogr.,* **30,** 1776–1789.

Sutton, R. T., and M. R. Allen, 1997: Decadal predictability of North Atlantic sea surface temperature and climate. *Nature,* **388,** 563–567.

Taylor, A. H., and J. A. Stephens, 1998: The North Atlantic oscillation and the latitude of the Gulf Stream. *Tellus,* **50A,** 134–142.

Weng, W., and D. Neelin, 1998: On the role of the ocean–atmosphere in midlatitude interdecadal variability. *Geophys. Res. Lett.,* **25,** 167–170.

White, W. B., Y. Chao, and C.-K. Tai, 1998: Coupling of the biennal oceanic Rossby wave with the overlying atmosphere in the Pacific basin. *J. Phys. Oceanogr.,* **28,** 123–1251.

Wunsch, C., 1999: The interpretation of short climate records, with comments on the North Atlantic and Southern Oscillations. *Bull. Amer. Meteor. Soc.,* **80,** 245–255.

Xu, W., T. P. Barnett, and M. Latif, 1998: Decadal variability in the North Pacific as simulated by a hybrid coupled model. *J. Climate,* **11,** 297–312.

Zorita, E., and C. Frankignoul, 1997: Modes of the North Atlantic decadal variability in the ECHAM1/LSG coupled ocean–atmosphere general circulation model. *J. Climate,* **10,** 183–200.